Journal of Nonlinear Mathematical Physics (2025) 32:22
https://doi.org/10.1007/s44198-025-00272-x

RESEARCH ARTICLE

Exploration of Soliton Dynamics and Chaos in the Landau-Ginzburg-Higgs Equation Through Extended Analytical Approaches

Khush Bukht Mehdi[1] · Abd Allah A. Mousa[2] · Sajawal Abbas Baloch[3] · Ulviye Demirbilek[4] · Abdullatif Ghallab[5] · Imran Siddique[3,6] · Rana Muhammad Zulqarnain[7]

Received: 18 January 2025 / Accepted: 21 February 2025

Abstract

The goal of this work is to improve our understanding of the dynamical aspects of the nonlinear Landau-Ginzburg-Higgs (LGH) equation, which offers a theoretical framework for characterizing several phenomena, including the spontaneous breakdown of symmetries and the emergence of superconducting states. The proposed model integrates the concepts of the Higgs mechanism and the Landau-Ginzburg theory when symmetry breaking appears in phase transitions in particle physics or condensed matter systems. The equation is essential for describing the Higgs field and its constituent particles, such as the Higgs boson. New extended direct algebraic approaches and modified F-expansion techniques are used to address this problem. The obtained solutions, which include kink, anti-kink, bright, dark, and periodic solitons, are essential because they shed light on the stability and nonlinear dynamics of field theories that are pertinent to cosmology and condensed matter physics. To advance the essential propagating features, a few obtained solutions are presented as 3D, contour, and 2D graphics by applying certain values to the parameters under the given constraints. The dynamical insights are examined and significant aspects of the phenomenon under study are discussed through the use of the bifurcation analysis. Additionally, the chaos analysis is carried out to show the quasi-periodic and periodic chaotic patterns. The sensitivity analysis of the studied model is also looked at and presented at different initial conditions. Furthermore, we guarantee that every found solution is precise, effective, and a great addition to the literature of solitary wave theory. To calculate the soliton solutions for nonlinear models in communication engineering and operations research, the methods utilized in this work to derive inclusive and standard solutions are more accessible, effective, and quick.

Extended author information available on the last page of the article

Published online: 16 April 2025

Keywords Nonlinear evolution equations · New extended direct algebraic method · Modified F-expansion method · The LGH equation · Soliton solutions · Bifurcation analysis · Sensitivity analysis

1 Introduction

In many different fields, such as engineering, physics, and biology, nonlinear partial differential equations (NLPDEs) are essential for simulating distinct physical phenomena [1–8]. By taking nonlinearity into account and maintaining complicated dynamics, these equations describe intricate systems and processes. In fluid dynamics, NLPDEs are utilized to depict and evaluate fluid flow phenomena, such as modeling turbulent flow and investigating fluid-structure interactions. In the field of optics, NLPDEs are utilized to mathematically characterize and study nonlinear processes that transpire within optical systems. These phenomena have a broad range of applications, such as studying nonlinear optical systems, ultrashort pulse propagation characteristics, and nonlinear wave behavior [9–11]. The Korteweg-de Vries (KdV) model is a widely recognized model that represents wave motion in shallow canals. A nonlinear Schrädinger equation is the second one that arises in this area. The KdV equation is specifically regarded in this sense as a test problem for the recently suggested approach, which means that it is a solved equation with known behavior. Modeling, solving problems, and developing new methodologies depend not just on one field but also on other areas of mathematics and allied fields like physics, biology, optical physics, quantum, and so forth. A number of effective techniques have been reported in the literature to find the analytical solutions for nonlinear evolution equations (NLEEs) [12, 13], such as Hirota's bilinear technique [14], modified expansion function scheme [15], sine-cosine approach [16], tanh technique [17], exponential rational function approach [18], sine-Gordon expansion scheme [19], Improved Bernoulli Sub-Equation Function (IBSEF) method [20], modified extended tanh-function method and modified generalized Kudryashov method [21], extended hyperbolic function method [22], modified auxiliary equation method and Sardar sub-equation method [23], tanh-coth expansion approach [24, 25], first integral technique [26, 27], new auxiliary equation approach [28–30], modified simplest equation approach [31, 32], Riccati equation technique [33, 34], generalized Riccati equation mapping method[35], extended direct algebraic approach [36–38], Kudryashov scheme [39, 40], the modified extended exp-function technique [41, 42], the Backlund transformation method [43, 44], Jacobi elliptic function expansion approach [45, 46], modified Khater technique [47, 48], generalized exponential rational function approach [49, 50], and many more [51–56]. To the best of our understanding, there is a significant deficiency in substantial research regarding our suggested techniques for deriving the LGH equation. Additionally, the innovative extended direct algebraic method and the modified F–expansion method (MFEM) have proven to be exceptionally effective, offering a thorough and practical framework for achieving accurate solutions to NLPDEs in the context of traveling waves[57]. As a consequence of the previous research, the goal of this study is to use the proposed techniques to find soliton solutions of the LGH model. The ODE of a NLPDE can be solved analyti-

cally by integrating a transformation with a novel extended direct algebraic method and a modified F-expansion technique. These methods are particularly employed to address the nonlinear LGH equation. The primary advantages of the proposed methods lie in their analytical characteristics and their capacity to manage a wide range of nonlinear fractional differential equations. Additionally, the bifurcation analysis, sensitivity analysis, and chaotic behavior of the suggested model are also discussed. Stability and bifurcation analysis are crucial for comprehending the behavior of dynamic systems. This analysis offers a foundational framework for investigating intricate phenomena and dynamics across a range of scientific fields, including physics, reaction diffusion processes, chemical reactions, biology, engineering, economics, and numerous other areas. Furthermore, it assists in forecasting the long-term behavior of dynamical systems. In engineering, it is instrumental in the design and optimization of stable and resilient systems, such as electrical circuits, mechanical structures, and chemical processes. Stability analysis plays a crucial role in the design and regulation of systems, ensuring their stability and mitigating undesirable behaviors such as oscillations, instabilities, or chaotic dynamics. Conversely, bifurcation analysis investigates the qualitative transformations that a system experiences as a parameter is altered. This analysis reveals critical parameter values at which the system transitions, leading to the emergence of new equilibrium points or the onset of intricate dynamics, including chaos. Through the examination of stability and bifurcations, researchers acquire significant insights into the behavior and stability of dynamical models, facilitating a more profound comprehension of complex systems across various scientific fields. Different wave solitons are formed by inserting specified values of arbitrary components, and these achieved solitons have not been reported in the prior literature. In comparison with the previously researched methodologies, the current methodology performs more effectively and efficiently and offers more broad solutions. By employing the suggested techniques, the solitonic structures of the LGH equation have been effectively demonstrated and the TWs have provided exact solutions. The uniqueness of the obtained results is provided and the survey results are contrasted with the highly regarded outcomes. We are confident that our efforts will enable physicists to predict new concepts in mathematical physics. The LGH equation is given as: [57]

$$\frac{\partial^2 u}{\partial t^2} - \frac{\partial^2 u}{\partial x^2} - m^2 u + n^2 u^3 = 0, \tag{1.1}$$

where $u(x, t)$ is the ion-cyclotron wave's electrostatic potential, m and n are real parameters, x and t represent the nonlinear spatial and temporal coordinates. In physics, the LGH system is a theoretical framework that combines the Higgs mechanism and the Landau-Ginzburg theory. In the 1950s, Lev Landau and Alexei Ginzburg developed the Landau-Ginzburg theory to give a phenomenological understanding of phase transitions, particularly in superconductors. To describe the conversion of a normal to a superconducting state, an order parameter has been introduced. In 1964, Peter Higgs and several physicists, including Robert Brout and Francois Englert, suggested the Higgs mechanism, which explains how particles gain mass. The mechanism relies on the spontaneous breaking of symmetry and the collision of a scalar

field (Higgs field) with particles, which results in the production of particle masses. When Landau-Ginzburg theory and the Higgs mechanism were combined in the 1970s, the LGH structure was created. This conceptual framework is particularly relevant for particle physics and the investigation of phase transitions in certain condensed matter systems.

The ability of NLPDEs to provide profound insights into the behavior of intricate physical phenomena makes their accurate solution extremely important [58, 59]. In many scientific fields, such as physics, engineering, biology, and finance, NLPDEs are commonly encountered because linear approximations are not always sufficient to explain the complexities of real-world systems. The utilization of exact solutions facilitates the understanding of the underlying principles guiding the system by offering a detailed mathematical depiction of its dynamics. Additionally, these solutions enable the validation of computational models by acting as standards for approximate approaches and numerical simulations. Finding exact solutions also aids in the creation of novel mathematical methods and instruments, which advances our knowledge of nonlinear processes and offers new avenues for creative scientific and technological applications [60, 61]. To assess the unique soliton solutions to the integrable NLEE (1.1), various techniques have been used. Bekir and Unsal [62] found several solutions for exponential functions by exploring the NLEE (1.1) using the first integral approach. Iftikhar et al. [63] used the $\left(\frac{G'}{G}, \frac{1}{G}\right)$-expansion technique to investigate various types of analytical solutions to NLEE (1.1). They have determined kink shape soliton and general soliton solutions for various parametric choices. By employing the IBSEF approach, Islam and Akbar [64] obtained a few different kinds of solutions. In this work, we utilized two efficient analytical approaches to find the soliton solutions of proposed model. Several authors have developed these two proposed techniques to ascertain the exact solutions of various Nonlinear Evolution Equations (NLEEs). However, there has been no successful application of these methods to our preferred LGH equation. In this context, the new exact solution we have identified for the LGH equation is more accurate, efficient, and accessible. These solutions can be applied across multiple domains, including computational physics, engineering, and areas related to wave analysis. The acquired results offer a variety of soliton shapes, including periodic, kink wave, singular, and other shapes that help in understanding the dynamical behaviour of governing systems. The remainder of the article is organized as follows: In section 2, we present algorithms of analytical techniques, and in section 3, the application of the LGH equation is provided. In sections 4, 5 and 6, we study the dynamical behavior of the LGH equation, containing the phase portraits, chaos, and sensitivity analysis using dynamical systems respectively. The results and discussion are presented in Section 7. A detailed evaluation of previous studies is provided in Section 8, while the conclusion is presented in Section 9.

2 Algorithm of the Schemes

2.1 The New Extended Direct Algebraic Method

A thorough description of the primary steps involved in the new extended direct algebraic method is given in this section.

Step 1.

Let us consider NLPDE of the following form

$$F(w, w_t, w_x, w_{tt}, w_{xx}, ...) = 0. \tag{2.1}$$

By utilizing the transformation

$$w(x,t) = U(\psi) = x - ct, \tag{2.2}$$

where $c \neq 0$, and we obtain ordinary differential equation (ODE) of the form

$$G(U, U', U'', ...) = 0. \tag{2.3}$$

Step 2.

By assuming the following solution of the ODE as

$$U = U(\psi) = \sum_{j=0}^{K} a_j Z^j(\psi), \tag{2.4}$$

where $a_j (j = 0, 1, 2, ...K)$ are constant coefficients to be found and $Z(\psi)$ satisfies the ODE of the form

$$Z'(\psi) = ln(\rho)\left(\chi + vW(\psi) + \lambda W^2(\psi)\right), \rho \neq 0, 1. \tag{2.5}$$

Here v, χ, along with λ are the real constants that can be seen in the auxiliary equation. The list of numerous solutions is exposed below [65].

Family-1 When $\phi < 0$ and $\lambda \neq 0$, where $\phi = v^2 - 4\chi\lambda$,

$$\begin{cases} Z_1(\psi) = -\frac{v}{2\lambda} + \frac{\sqrt{-\phi}}{2\lambda}\tan_\rho\left(\frac{\sqrt{-\phi}}{2}\psi\right), \\ Z_2(\psi) = -\frac{v}{2\lambda} + \frac{\sqrt{-\phi}}{2\lambda}\cot_\rho\left(\frac{\sqrt{-\phi}}{2}\psi\right), \\ Z_3(\psi) = -\frac{v}{2\lambda} + \frac{\sqrt{-\phi}}{2\lambda}\left(\tan_\rho\left(\sqrt{-\phi}\psi\right) \pm \sqrt{gh}\sec_\rho\left(\sqrt{-\phi}\psi\right)\right), \\ Z_4(\psi) = -\frac{v}{2\lambda} + \frac{\sqrt{-\phi}}{2\lambda}\left(\cot_\rho\left(\sqrt{-\phi}\psi\right) \pm \sqrt{gh}\csc_\rho\left(\sqrt{-\phi}\psi\right)\right), \\ Z_5(\psi) = -\frac{v}{2\lambda} + \frac{\sqrt{-\phi}}{4\lambda}\left(\tan_\rho\left(\frac{\sqrt{-\phi}}{4}\psi\right) - \cot_\rho\left(\frac{\sqrt{-\phi}}{4}\psi\right)\right). \end{cases}$$

Family-2 When $\phi > 0$ and $\lambda \neq 0$,

$$\begin{cases} Z_6(\psi) = -\frac{v}{2\lambda} - \frac{\sqrt{-\phi}}{2\lambda}\tanh_\rho\left(\frac{\sqrt{\phi}}{2}(\psi)\right), \\ Z_7(\psi) = -\frac{v}{2\lambda} - \frac{\sqrt{-\phi}}{2\lambda}\coth_\rho\left(\frac{\sqrt{\phi}}{2}(\psi)\right), \\ Z_8(\psi) = -\frac{v}{2\lambda} + \frac{\sqrt{\phi}}{2\lambda}\left(-\tanh_\rho\left(\sqrt{-\phi}\psi\right) \pm i\sqrt{gh}\mathrm{sech}_\rho\left(\sqrt{\phi}\psi\right)\right), \\ Z_9(\psi) = -\frac{v}{2\lambda} + \frac{\sqrt{\phi}}{2\lambda}\left(-\coth_\rho\left(\sqrt{-\phi}\psi\right) \pm i\sqrt{gh}\mathrm{csch}_\rho\left(\sqrt{\phi}\psi\right)\right), \\ Z_{10}(\psi) = -\frac{v}{2\lambda} - \frac{\sqrt{\phi}}{4\lambda}\left(\tanh_\rho\left(\frac{\sqrt{\phi}}{4}\psi\right) - \coth_\rho\left(\frac{\sqrt{\phi}}{4}\psi\right)\right). \end{cases}$$

Family-3 When $\chi\lambda > 0$ and $v = 0$,

$$\begin{cases} Z_{11}(\psi) = \sqrt{\frac{\chi}{\lambda}}\tan_\rho\left(\sqrt{\chi\lambda}\psi\right), \\ Z_{12}(\psi) = -\sqrt{\frac{\chi}{\lambda}}\cot_\rho\left(\sqrt{\chi\lambda}\psi\right), \\ Z_{13}(\psi) = \sqrt{\frac{\chi}{\lambda}}\left(\tan_\rho\left(2\sqrt{\chi\lambda}\psi\right) \pm \sqrt{gh}\sec_\rho\left(2\sqrt{\chi\lambda}\psi\right)\right), \\ Z_{14}(\psi) = \sqrt{\frac{\chi}{\lambda}}\left(-\cot_\rho\left(2\sqrt{\chi\lambda}\psi\right) \pm \sqrt{gh}\csc_\rho\left(2\sqrt{\chi\lambda}\psi\right)\right), \\ Z_{15}(\psi) = \frac{1}{2}\sqrt{\frac{\chi}{\lambda}}\left(\tan_\rho\left(\frac{\sqrt{\chi\lambda}}{2}\psi\right) - \cot\left(\frac{\sqrt{\chi\lambda}}{2}\psi\right)\right). \end{cases}$$

Family-4 When $\chi\lambda < 0$ and $v = 0$,

$$\begin{cases} Z_{16}(\psi) = -\sqrt{-\frac{\chi}{\lambda}}\tanh_\rho\left(\sqrt{-\chi\lambda}\psi\right), \\ Z_{17}(\psi) = -\sqrt{-\frac{\chi}{\lambda}}\coth_\rho\left(\sqrt{-\chi\lambda}\psi\right), \\ Z_{18}(\psi) = \sqrt{-\frac{\chi}{\lambda}}\left(-\tanh_\rho\left(2\sqrt{-\chi\lambda}\psi\right) \pm i\sqrt{gh}\mathrm{sech}_\rho\left(2\sqrt{-\chi\lambda}\psi\right)\right), \\ Z_{19}(\psi) = \sqrt{-\frac{\chi}{\lambda}}\left(-\coth_\rho\left(2\sqrt{-\chi\lambda}\psi\right) \pm i\sqrt{gh}\mathrm{csch}_\rho\left(2\sqrt{-\chi\lambda}\psi\right)\right), \\ Z_{20}(\psi) = -\frac{1}{2}\sqrt{-\frac{\chi}{\lambda}}\left(\tanh_\rho\left(\frac{\sqrt{-\chi\lambda}}{2}\psi\right) + \coth_\rho\left(\frac{\sqrt{-\chi\lambda}}{2}\psi\right)\right). \end{cases}$$

Family-5 When $v = 0$ and $\chi = \lambda$,

$$\begin{cases} Z_{21}(\psi) = \tan_\rho(\chi(\psi)), \\ Z_{22}(\psi) = -\cot_\rho(\chi(\psi)), \\ Z_{23}(\psi) = \tan_\rho(2\chi(\psi)) \pm \sqrt{gh}\sec_\rho(2\chi\psi), \\ Z_{24}(\psi) = -\cot_\rho(2\chi(\psi)) \pm \sqrt{gh}\csc_\rho(2\chi\psi), \\ Z_{25}(\psi) = \frac{1}{2}\left(\tan_\rho\left(\frac{\chi}{2}\psi\right) - \cot_\rho\left(\frac{\chi}{2}\psi\right)\right). \end{cases}$$

Family-6 When $v = 0$ and $\chi = -\lambda$,

$$\begin{cases} Z_{26}(\psi) = -\tanh_\rho(\chi\psi), \\ Z_{27}(\psi) = -\coth_\rho(\chi\psi), \\ Z_{28}(\psi) = -\tanh_\rho(2\chi\psi) \pm i\sqrt{gh}\mathrm{sech}_\rho(2\chi\psi), \\ Z_{29}(\psi) = -\coth_\rho(2\chi\psi) \pm \sqrt{gh}\mathrm{csch}_\rho(2\chi\psi), \\ Z_{30}(\psi) = -\frac{1}{2}\tanh_\rho\left(\frac{\psi}{2}\chi\right) + \coth_\rho\left(\frac{\psi}{2}\chi\right). \end{cases}$$

Family-7 When $v^2 = 4\chi\lambda$,

$$Z_{31} = \frac{-2\chi(v\psi \ln \rho + 2)}{v^2(\psi) \ln \rho}.$$

Family-8 When $v = p, \chi = pq, (q \neq 0)$ and $\lambda = 0$,

$$Z_{32} = \rho^{p(\psi)} - q.$$

Family-9 When $v = \lambda = 0$,

$$Z_{33} = \chi(\psi) \ln \rho.$$

Family-10 When $v = \chi = 0$,

$$Z_{34}(\psi) = \frac{-1}{\zeta\psi \ln \rho}.$$

Family-11 When $\chi = 0$ and $v \neq 0$,

$$\begin{cases} Z_{35} = -\frac{gv}{\lambda(\cosh_\rho(v\psi) - \sinh_\rho(v\psi) + g)}, \\ Z_{36} = -\frac{v(\sinh_\rho(v\psi) + \cosh_\rho(v\psi))}{\lambda(\sinh_\rho(v\psi) + \cosh_\rho(v\psi) + h)}. \end{cases}$$

Family-12 When $v = p$, $\lambda = pq$,$(q \neq 0, \chi = 0)$,

$$Z_{37} = -\frac{g\rho^{p\psi}}{g - qh\rho^{p\psi}}.$$

Now, the hyperbolic and trigonometric functions are given as follows:

$$\begin{cases} \sinh_\rho(\psi) = \frac{g\rho^{\psi} - h\rho^{-\psi}}{2}, \\ \cosh_\rho(\psi) = \frac{g\rho^{\psi} + h\rho^{-\psi}}{2}, \\ \tanh_\rho(\psi) = \frac{g\rho^{\psi} - h\rho^{-\psi}}{g\rho^{\psi} + h\rho^{-\psi}}, \\ \coth_\rho(\psi) = \frac{g\rho^{\psi} + h\rho^{-\psi}}{g\rho^{\psi} - h\rho^{-\psi}}, \\ \operatorname{sech}_\rho(\psi) = \frac{2}{g\rho^{\psi} + h\rho^{-\psi}}, \\ \operatorname{csch}_\rho(\psi) = \frac{2}{g\rho^{\psi} - h\rho^{-\psi}}, \\ \sin_\rho(\psi) = \frac{g\rho^{i\psi} - h\rho^{-i\psi}}{2i}, \\ \cos_\rho(\psi) = \frac{g\rho^{i\psi} + h\rho^{-i\psi}}{2}, \\ \tan_\rho(\psi) = -i\frac{g\rho^{i\psi} - h\rho^{-i\psi}}{g\rho^{i\psi} + h\rho^{-i\psi}}, \\ \cot_\rho(\psi) = i\frac{g\rho^{i\psi} + h\rho^{-i\psi}}{g\rho^{i\psi} - h\rho^{-i\psi}}, \\ \sec_\rho(\psi) = \frac{2}{g\rho^{i\psi} + h\rho^{-i\psi}}, \\ \csc_\rho(\psi) = \frac{2i}{g\rho^{i\psi} - h\rho^{-i\psi}}, \end{cases}$$

where $g, h > 0$ are called parameters of deformation. By balancing the highest-order derivative term with the highest-order nonlinear term in Eq. (2.2), we may get the value of K. The set of algebraic equations can be obtained by substituting Eq. (2.4) and its necessary derivatives in Eq. (2.2) and comparing the coefficients of power of $Z(\psi)$ in the resulting equation.

2.2 The Modified *F*-Expansion Method

The main steps of the MFEM are given [66–68].

$$U(\psi) = a_0 + \sum_{i=1}^{m} a_1 F^i(\psi) + \sum_{i=1}^{m} b_1 F^{-i}(\psi), \tag{2.6}$$

where a_0, a_i and b_i are real parameters to be determined. $F(\psi)$ satisfies the nonlinear ODE of the form:

$$F'(\psi) = Q + RF(\psi) + SF^2(\psi), \tag{2.7}$$

where Q, R and S are constants given in Table 1. The determination of an integer m can be achieved by using the balancing principle.

Eq. (2.7) yields the distinct Riccati function solution $F(\psi)$, by giving distinct values of Q, R, and S (see Table 1).

Step 1: By assuming the Eqs. (2.1), (2.2), and (2.3).
Step 2: Expand the solution to Eq. (2.3).
Step 3: An algebraic system of equations for a_i and b_i can be obtained by replacing Eq. (2.7) and Eq. (2.6) into Eq. (2.3) and collecting coefficients of $F^i(\psi)$ to zero.

Table 1 Relations between Q, R, and S with F

Q	R	S	$F(\psi)$
Q = 0	R = 1	S = - 1	$\frac{1}{2} + \frac{1}{2}\tanh(\frac{\psi}{2})$
Q = 0	R = - 1	S = 1	$\frac{1}{2} - \frac{1}{2}\coth(\frac{\psi}{2})$
Q = $\frac{1}{2}$	R = 0	S = - $\frac{1}{2}$	$\coth(\psi) \pm csch(\psi)$, $\tanh(\psi) \pm i\,\mathrm{sech}(\psi)$
Q = 1	R = 0	S = - 1	$\tanh(\psi)$, $\coth(\psi)$
Q = $\frac{1}{2}$	R = 0	$S = \frac{1}{2}$	$\sec(\psi) + \tan(\psi)$, $\csc(\psi) - \cot(\psi)$
Q = -$\frac{1}{2}$	R = 0	S = -$\frac{1}{2}$	$\sec(\psi) - \tan(\psi)$, $\csc(\psi) + \cot(\psi)$
Q = - 1	R = 0	S = - 1	$\tan(\psi)$, $\cot(\psi)$
Q =0	R = 0	S $\neq$ 0	$\frac{1}{S\psi+\varepsilon}$, ε is arbitrary constant
Arbitrary constant	R = 0	S = 0	$Q\psi$
Arbitrary constant	R $\neq$ 0	S = 0	$\frac{(-Q+\exp(R\psi)}{R}$

Step 4: Utilizing MATHEMATICA, solve the system of algebraic equations. By inserting these findings into Equation (2.7), we can derive the general structure of TWs for Eq. (2.3).

Step 5: Several soliton-like solutions, solutions for trigonometric functions, and rational solutions to Eq. (2.1) may be found by taking Q, R, S and $F(\psi)$ from Table 1 and inserting them into Eq. (2.6) along with a_i and b_i. More rich forms of solutions to the NLPDEs will be obtained using this approach. It demonstrates that the MFEM is more effective at creating exact solutions for NLPDEs.

3 Application of the Techniques

Let us take the transformation of the form:

$$U(x,t) = U(\psi), \psi = x - ct. \tag{3.1}$$

By using Eq. (3.1) into Eq. (1.1), we obtain the subsequent ODE

$$c^2U'' - U'' - m^2U + n^2U^3 = 0, \tag{3.2}$$

where m, c, and n are free parameters.

3.1 Solutions with New Extended Direct Algebraic Method

Using the homogeneous balancing method between U'' and U^3 in Eq. (3.2), we obtain $N = 1$. Consequently, the solution form can be represented as

$$U(\psi) = a_0 + a_1 Z(\psi), \tag{3.3}$$

where a_0 and a_1 are unknown parameters. The set of equations involving a_0, a_1, and other parameters is obtained by summing up all the coefficients of distinct powers of $Z(\psi)$ and combining Eqs. (3.3) and (2.5) into Eq. (3.2). The following outcomes are obtained by solving these equations:

$$a_0 = \Delta v, a_1 = 2\Delta\lambda, m = \Delta n\sqrt{\phi}, \phi = v^2 - 4\chi\lambda, \tag{3.4}$$

where $\Delta = \frac{\sqrt{1-c^2}}{\sqrt{2}n}$.

The solution to Eq. (3.2), which corresponds to (3.4), can be determined as follows, accordingly.

Set 1. When $\phi < 0$ and $\lambda \neq 0$, then

$$\begin{cases} u_1 = \Delta\sqrt{-\phi}\tan_\rho\left(\frac{\sqrt{-\phi}}{2}\psi\right), \\ u_2 = -\Delta\sqrt{-\phi}\cot_\rho\left(\frac{\sqrt{-\phi}}{2}\psi\right), \\ u_3 = \Delta\sqrt{-\phi}\left(\tan_\rho\left(\sqrt{-\phi}\psi\right) \pm \sqrt{gh}\sec_\rho\left(\sqrt{-\phi}\psi\right)\right), \\ u_4 = \Delta\sqrt{-\phi}\left(\cot_\rho\left(\sqrt{-\phi}\psi\right) \pm \sqrt{gh}\csc_\rho\left(\sqrt{-\phi}\psi\right)\right), \\ u_5 = \Delta\frac{\sqrt{-\phi}}{2}\left(\tan_\rho\left(\frac{\sqrt{-\phi}}{4}\psi\right) - \cot_\rho\left(\frac{\sqrt{-\phi}}{4}\psi\right)\right). \end{cases} \tag{3.5}$$

Set-2 When $\phi > 0$ and $\lambda \neq 0$, then

$$\begin{cases} u_6 = -\Delta\sqrt{-\phi}\tanh_\rho\left(\frac{\sqrt{\phi}}{2}\psi\right), \\ u_7 = -\Delta\sqrt{-\phi}\coth_\rho\left(\frac{\sqrt{\phi}}{2}\psi\right), \\ u_8 = \Delta\sqrt{\phi}\left(-\tanh_\rho\left(\sqrt{-\phi}\psi\right) \pm i\sqrt{gh}\operatorname{sech}_\rho\left(\sqrt{\phi}\psi\right)\right), \\ u_9 = -\Delta\sqrt{\phi}\left(-\coth_\rho\left(\sqrt{-\phi}\psi\right) \pm i\sqrt{gh}\operatorname{csch}_\rho\left(\sqrt{\phi}\psi\right)\right), \\ u_{10} = -\Delta\frac{\sqrt{\phi}}{2}\left(\tanh_\rho\left(\frac{\sqrt{\phi}}{4}\psi\right) - \coth_\rho\left(\frac{\sqrt{\phi}}{4}\psi\right)\right). \end{cases} \tag{3.6}$$

Set-3 When $\chi\lambda > 0$ and $v = 0$, then

$$\begin{cases} u_{11} = 2\Delta\sqrt{\chi\lambda}\tan_\rho\left(\sqrt{\chi\lambda}\psi\right), \\ u_{12} = -2\Delta\sqrt{\chi\lambda}\cot_\rho\left(\sqrt{\chi\lambda}\psi\right), \\ u_{13} = 2\Delta\sqrt{\chi\lambda}\left(\tan_\rho\left(2\sqrt{\chi\lambda}\psi\right) \pm \sqrt{gh}\sec_\rho\left(2\sqrt{\chi\lambda}\psi\right)\right), \\ u_{14} = 2\Delta\sqrt{\chi\lambda}\left(-\cot_\rho\left(2\sqrt{\chi\lambda}\psi\right) \pm \sqrt{gh}\csc_\rho\left(2\sqrt{\chi\lambda}\psi\right)\right), \\ u_{15} = \Delta\sqrt{\chi\lambda}\left(\tan_\rho\left(\frac{\sqrt{\chi\lambda}}{2}\psi\right) - \cot\left(\frac{\sqrt{\chi\lambda}}{2}\psi\right)\right). \end{cases} \tag{3.7}$$

Set-4 When $\chi\lambda < 0$ and $v = 0$, then

$$\begin{cases} u_{16} = -2i\Delta\sqrt{\chi\lambda}\tanh_\rho\left(\sqrt{-\chi\lambda}\psi\right), \\ u_{17} = -2i\Delta\sqrt{\chi\lambda}\coth_\rho\left(\sqrt{-\chi\lambda}\psi\right), \\ u_{18} = -2i\Delta\sqrt{\chi\lambda}\left(-\tanh_\rho\left(2\sqrt{-\chi\lambda}\psi\right) \pm i\sqrt{gh}\operatorname{sech}_\rho\left(2\sqrt{-\chi\lambda}\psi\right)\right), \\ u_{19} = -2i\Delta\sqrt{\chi\lambda}\left(-\coth_\rho\left(2\sqrt{-\chi\lambda}\psi\right) \pm i\sqrt{gh}\operatorname{csch}_\rho\left(2\sqrt{-\chi\lambda}\psi\right)\right), \\ u_{20} = -\Delta i\sqrt{\chi\lambda}\left(\tanh_\rho\left(\frac{\sqrt{-\chi\lambda}}{2}\psi\right) + \coth_\rho\left(\frac{\sqrt{-\chi\lambda}}{2}\psi\right)\right). \end{cases} \tag{3.8}$$

Set-5 When $v = 0$ and $\chi\lambda$, then

$$\begin{cases} u_{21} = 2\Delta\lambda\tan_\rho(\chi\psi), \\ u_{22} = -2\Delta\lambda\cot_\rho(\chi\psi), \\ u_{23} = 2\Delta\lambda\left(\tan_\rho(2\chi\psi) \pm \sqrt{gh}\sec_\rho(2\chi\psi)\right), \\ u_{24} = 2\Delta\lambda\left(-\cot_\rho(2\chi\psi) \pm \sqrt{gh}\csc_\rho(2\chi\psi)\right), \\ u_{25} = \Delta\lambda\left(\tan_\rho\left(\frac{\chi}{2}\psi\right) - \cot_\rho\left(\frac{\chi}{2}\psi\right)\right). \end{cases} \tag{3.9}$$

Set-6 When $v = 0$ and $\chi = -\lambda$, then

$$\begin{cases} u_{26} = 2\Delta\mu\tanh_\rho(\chi\psi), \\ u_{27} = 2\Delta\mu\coth_\rho(\chi\psi), \\ u_{28} = -2\Delta\chi\left(-\tanh_\rho(2\chi\psi) \pm i\sqrt{gh}\operatorname{sech}_\rho(2\chi\psi)\right), \\ u_{29} = -2\Delta\chi\left(-\coth_\rho(2\chi\psi) \pm i\sqrt{gh}\operatorname{csch}_\rho(2\chi\psi)\right), \\ u_{30} = \Delta\chi\left(\tanh_\rho\left(\frac{\chi}{2}\psi\right) \pm \coth_\rho\left(\frac{\chi}{2}\psi\right)\right). \end{cases} \tag{3.10}$$

Set-7 When $v^2 = 4\chi\lambda$, then

$$u_{31} = 2\Delta\chi\lambda\left(\frac{1}{\sqrt{\chi\lambda}} - \frac{2\chi(v\psi\ln\rho + 2)}{v^2\psi\ln\rho}\right). \tag{3.11}$$

Set-8 When $v = \mu = 0$, then

$$u_{32} = \frac{-2\Delta}{\psi\ln\rho}. \tag{3.12}$$

Set-9 When $\chi = 0$ and $v \neq 0$, then

$$\begin{cases} u_{33} = \Delta v\left(1 - \frac{2g}{(\cosh_\rho(v\psi) - \sinh_\rho(v\psi) + g)}\right), \\ u_{34} = \Delta v\left(1 - \frac{2(\sinh_\rho(v\psi) + \cosh_\rho(v\psi))}{\lambda(\sinh_\rho(v\psi) + \cosh_\rho(v\psi) + h)}\right). \end{cases} \tag{3.13}$$

Set-10 When $v = p$, $\lambda = pq$, and $(q \neq 0, \chi = 0)$, then

$$u_{35} = -\frac{g\rho^{p\psi}}{g - qh\rho^{p\psi}}. \tag{3.14}$$

3.2 Solutions with the Modified *F* Expansion Method

We get $N = 1$ from Eq. 3.2 by applying the homogeneous balancing approach between U'' and U^3. For $N = 1$, Eq. (2.6) becomes:

$$U(\psi) = a_0 + a_1F + \frac{b_1}{F}, \tag{3.15}$$

where a_0 and a_1 are real constants. Inserting Eqs. (3.15) and (2.7) into Eq. (3.2) and adding up all the coefficients of different powers of $Z(\eta)$ allows us to derive the system of equations including a_0, a_1, and other parameters. By solving these equations, we arrive at the subsequent results:

$$\begin{cases} a_0 = \Delta v, \\ a_1 = 2\Delta\lambda, \\ m = \Delta n\sqrt{\phi}, \\ \phi = v^2 - 4\chi\lambda, \end{cases} \tag{3.16}$$

where $\Delta = \frac{\sqrt{1-c^2}}{\sqrt{2}n}$.

Using Eq. (3.15) into Eq. (3.2) along with the solution of Eq. (2.7), we obtain

$$Q = 0, R = 1, S = -1.$$

$$a_0 = \frac{m}{n}, a_1 = -\frac{2m}{n}, b_1 = 0, c = \sqrt{1-2m}. \tag{3.17}$$

Put Eq. (3.17) into Eq. (3.15) along with the solution of Eq. (2.7), we get

$$u_1 = -\frac{m}{n}\tanh\left(\frac{\psi}{2}\right). \tag{3.18}$$

For $Q = 0, R = -1, S = 1$.

$$a_0 = -\frac{m}{n}, a_1 = \frac{2m}{n}, b_1 = 0, c = -\sqrt{1-2m}.$$

$$u_2 = -\frac{m}{n}\coth\left(\frac{\psi}{2}\right). \tag{3.19}$$

For $Q = \frac{1}{2}, R = 0, S = -\frac{1}{2}$.

$$a_0 = 0, a_1 = 0, b_1 = -\frac{m}{n}, c = \sqrt{1-2m}. \tag{3.20}$$

$$u_3 = -\frac{m}{n}\left(\frac{1}{(\coth(\psi) + \operatorname{csch}(\psi))}\right). \tag{3.21}$$

For $Q = 1, R = 0, S = -1$.

Family-1

$$a_0 = 0, a_1 = \frac{m}{2n}, b_1 = \frac{m}{2n}, c = -\frac{\sqrt{8-m^2}}{2\sqrt{2}}. \tag{3.22}$$

$$u_4 = \frac{m}{2n}\left(\tanh(\psi) + \frac{1}{\tanh(\psi)}\right). \tag{3.23}$$

Family-2

$$a_0 = 0, a_1 = 0, b_1 = -\frac{m}{n}, c = -\frac{\sqrt{2-m^2}}{\sqrt{2}}. \tag{3.24}$$

$$u_5 = -\frac{m}{n}\left(\frac{1}{\tanh(\psi)}\right). \tag{3.25}$$

For $Q = S = \frac{1}{2}, R = 0$.

$$a_0 = 0, a_1, = 0, b_1 = -\frac{im}{n}, c = \sqrt{1+2m^2}. \tag{3.26}$$

$$u_6 = -\frac{im}{n}\left(\frac{1}{(\tan(\psi) + \sec(\psi))}\right). \tag{3.27}$$

For $Q = S = -\frac{1}{2}, R = 0$.

$$a_0 = 0, a_1, = 0, b_1 = \frac{im}{n}, c = -\sqrt{1+2m^2}. \tag{3.28}$$

$$u_7 = \frac{im}{n}\left(\frac{1}{(\sec(\psi) + \tan(\psi))}\right). \tag{3.29}$$

For $Q = S = -1, R = 0$.

$$a_0 = 0, a_1, = -\frac{m}{\sqrt{2}n}, b_1 = \frac{m}{\sqrt{2}n}, c = -\frac{1}{2}\sqrt{4-m^2}. \tag{3.30}$$

$$u_8 = -\frac{m}{\sqrt{2}n}\left(\cot(\psi) - \frac{1}{\cot(\psi)}\right). \tag{3.31}$$

For $Q = 0, R = 0$.

$$a_0 = 0, a_1, = -\frac{\sqrt{2}S\sqrt{1-c^2}}{n}, b_1 = 0, m = 0. \tag{3.32}$$

$$u_9 = \frac{2S\sqrt{1-c^2}}{n(S\psi + \varepsilon)}. \tag{3.33}$$

For $R = 0, S = 0$.

$$a_0 = 0, a_1, = 0, b_1 = -\frac{\sqrt{2}Q\sqrt{1-c^2}}{n}, m = 0. \tag{3.34}$$

$$u_{10} = \frac{\sqrt{2}A\sqrt{1-c^2}}{n(Q\psi)}. \tag{3.35}$$

For $S = 0$.

$$a_0 = -\frac{m}{n}, a_1, = 0, b_1 = -\frac{2Qm}{Rn}, c = \frac{\sqrt{R^2-2m^2}}{R}. \tag{3.36}$$

$$u_{11} = -\frac{m}{n}\left(1 + \frac{2Q}{(e^{R\psi} - Q)}\right). \tag{3.37}$$

4 Qualitative Dynamics

Bifurcation is a phenomenon in dynamic systems where small changes in parameters lead to fundamental qualitative changes in the behavior of the system. This process often facilitates the emergence of new stable states, periodic orbits, or chaotic dynamics. Bifurcation theory provides information on the underlying mechanisms driving these abrupt transitions and enables the prediction of system behavior under different conditions. In this study, a comprehensive perspective on the bifurcation and phase diagrams of the proposed planner dynamic framework is presented. The suggested methodology, known for its versatility, offers a robust tool for the qualitative analysis of nonlinear models. Within this framework, a broad set of trajectories can be identified, ranging from points to simple closed curves and various other geometries. These trajectories represent diverse solution forms of Eq. (1.1) across different physical contexts.

Taking into account $\frac{dU}{d\psi}$, the dynamic framework for the planner concerning Eq. (3.2) can be expressed as follows:

$$\begin{cases} \dfrac{dU(\psi)}{d\psi} = V, \\ \dfrac{dV(\psi)}{d\psi} = G_1 U^3(\psi) - G_2 U(\psi), \end{cases} \tag{4.1}$$

where $G_1 = -\frac{n^2}{c^2-1}$ and $G_2 = \frac{m^2}{1-c^2}$. The Hamiltonian function is obtained by applying the first integral to Eq. (4.1)

$$H(U, V) = \frac{V^2}{2} - \frac{G_1 U^4}{4} + \frac{G_2 U^2}{2} = h, \tag{4.2}$$

where h denotes the constant total energy of the system. To determine the equilibrium points, the following system of equations is solved:

$$\begin{cases} V = 0, \\ G_1 U^3(\psi) - G_2 U(\psi) = 0. \end{cases} \tag{4.3}$$

The equilibrium points of Eq. (4.1) are determined by solving the system (4.3). This analysis reveals three potential equilibrium point scenarios, depending on the solutions of the equations.

The first solution, $U = 0$, always represents an equilibrium point corresponding to a trivial state where the system remains at rest. This point is denoted as:

$$H_1 = (0, 0).$$

The second type of solution arises from the quadratic equation $G_1 U^2 = G_2$, giving $U = \pm\sqrt{\frac{G_2}{G_1}}$.

The existence of these non-trivial equilibrium points depends on the sign of $\frac{G_2}{G_1}$. When G_1 and G_2 share the same sign, two symmetric equilibrium points exist, given by:

$$H_i = \left(\pm\sqrt{\frac{G_2}{G_1}}, 0 \right), \quad (i = 2, 3).$$

These points may correspond to stable or unstable states, depending on the potential function's nature. However, if G_1 and G_2 have opposite signs, $\frac{G_2}{G_1}$ becomes negative, and no real non-trivial equilibrium points exist.

The Jacobian matrix of the structure described by Eq. (4.3) is expressed with the following determinant form:

$$J(U, V) = \begin{vmatrix} 0 & 1 \\ 3G_1 U^2 - G_2 & 0 \end{vmatrix} = G_2 - 3G_1 U^2. \tag{4.4}$$

The equilibrium points are classified based on the value of the Jacobian determinant $J(U, V)$ as follows:

- Saddle Points $(J(U, V) < 0)$: When the Jacobian determinant is negative, the equilibrium points exhibit saddle-like behavior. This means the system is unstable in some directions and stable in others.
- Center Points $(J(U, V) > 0)$ 0)]]>: A positive Jacobian determinant corresponds to center points, where the system shows oscillatory or neutral stability, with trajectories forming closed loops around the equilibrium.
- Cuspid Points $(J(U, V) = 0)$: When the Jacobian determinant equals zero, the equilibrium points exhibit more complex nonlinear characteristics. Depending on the parameters G_1 and G_2, the dynamic behavior of the system is examined

in different regimes in terms of stable and unstable points, trajectory shapes, and transition behaviors as follows:

Case-1 By assigning specific parameter values $m = 3$, $c = 2$, and $n = 3$, we calculate $G_1 = -3$ and $G_2 = -3$. The system exhibits three equilibrium points:

$$H_1 = (0,0), \quad H_2 = \left(\sqrt{\frac{G_2}{G_1}}, 0\right) = (1,0), \text{and} \quad H_3 = \left(-\sqrt{\frac{G_2}{G_1}}, 0\right) = (-1,0).$$

The equilibrium point $H_1 = (0,0)$ is classified as a saddle point because $J(H_1) < 0$. In contrast, $H_2 = (1,0)$ is identified as a center point since $J(H_2) > 0$. Similarly, $H_3 = (-1,0)$ is also classified as a center point for $J(H_3) > 0$. These classifications are illustrated in Fig.1(a).

Case-2 Assigning specific values to the parameters $m = 0; c = 2; n = 1$, we obtain $G_1 = -0.333$ and $G_2 = 0$. The system has a equilibrium point: $H_1 = (0,0)$, For $J(H_1) = 0$, the equilibrium point $H_1 = (0,0)$ is classified as a cuspid point, as depicted in Fig.1(b).

Case-3 Assigning specific parameter values $m = 3$, $c = 0.5$, and $n = 1$, we compute $G_1 = 1.333$ and $G_2 = 12$. The system exhibits three equilibrium points:

$$H_1 = (0,0), \quad H_2 = \left(\sqrt{\frac{G_2}{G_1}}, 0\right) = (3,0), \text{and} \quad H_3 = \left(-\sqrt{\frac{G_2}{G_1}}, 0\right) = (-3,0).$$

The equilibrium point $H_1 = (0,0)$ is classified as a center since $J(H_1) > 0$. Meanwhile, $H_2 = (3,0)$ is identified as a saddle point due to $J(H_2) < 0$, and similarly, $H_3 = (-3,0)$ is classified as a saddle point for $J(H_3) < 0$. These classifications are illustrated in Fig.1(c).

5 Qualitative Dynamics Under Perturbation

The study of perturbed systems offers a comprehensive framework for exploring the intricate dynamics exhibited by nonlinear systems. This research employs advanced graphical methods, including 3D and 2D phase portraits, time series, and Poincaré sections, to systematically analyze the system's behavior across both stable and chaotic regimes. Such visualization techniques are instrumental in capturing the underlying dynamics of the system under varying conditions and in quantifying the influence of external perturbations. Notably, these analyses highlight the interplay between nonlinear structures and periodic forces, shedding light on their critical role in shaping the system's behavior. Within this framework, the following perturbed system is examined:

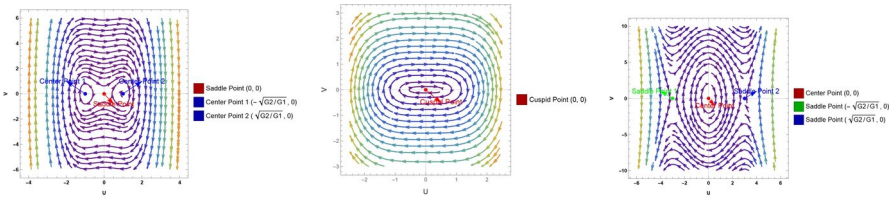

(a) $G_1 < 0, G_2 < 0$ (b) $G_1 < 0, G_2 = 0$ (c) $G_1 > 0, G_2 > 0$

Fig. 1 Phase portrait of the system (4.1)

$$\begin{cases} \dfrac{dU(\psi)}{d\psi} = V, \\ \dfrac{dV(\psi)}{d\psi} = G_1 U^3(\psi) - G_2 U(\psi) + \delta \cos(\sigma\psi), \end{cases} \tag{5.1}$$

where $\delta\cos(\sigma\psi)$ represents perturbation term. δ and σ signify the amplitude and the frequency of the system, respectively. This system combines the effects of external periodic forces and nonlinear interactions. In this study, the phase portraits, time series, and Poincaré sections of the system are analyzed in detail, and equilibrium points, periodic behaviors, and chaotic regimes are evaluated based on parameters and initial conditions through graphical analyses.

Remark 1 Figure 2 investigates the system with the parameters $G_1 = -3$, $G_2 = -3$ derived from $c = 2, m = 3, n = 3$, $\delta = 0.5$, and $\sigma = 1$. The 2D and 3D phase diagrams shown in (a) and (b) illustrate the chaotic behavior of the system. Additionally, the time series in (c) and the Poincaré sections in (d) confirm that the system operates within a chaotic regime, with no evidence of quasi-periodic structures.

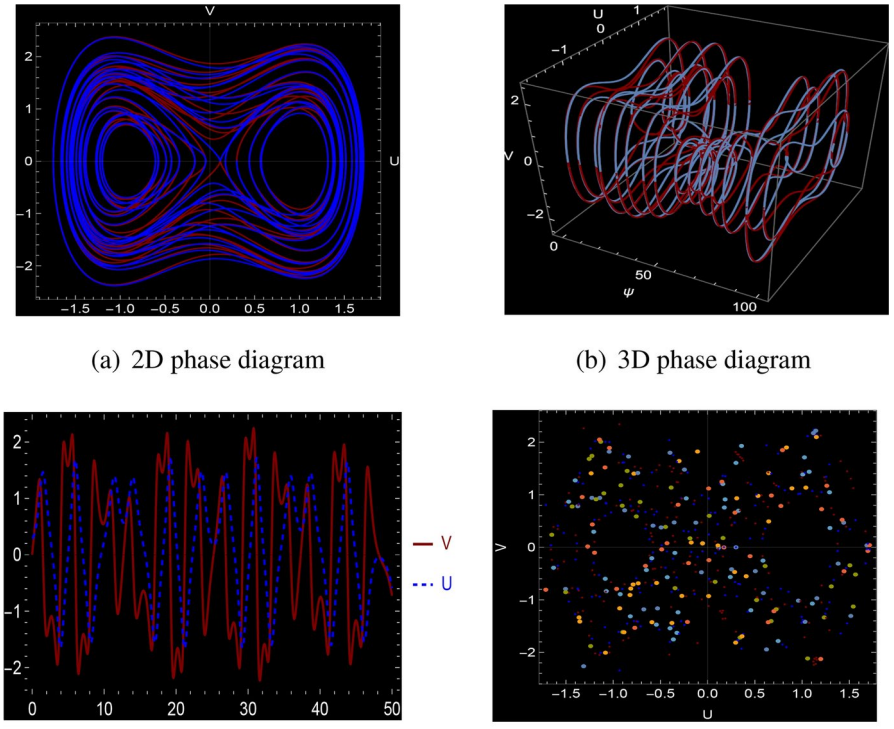

(a) 2D phase diagram

(b) 3D phase diagram

(c) Time series

(d) Poincaré section

Fig. 2 The chaotic behaviors of system (5.1)

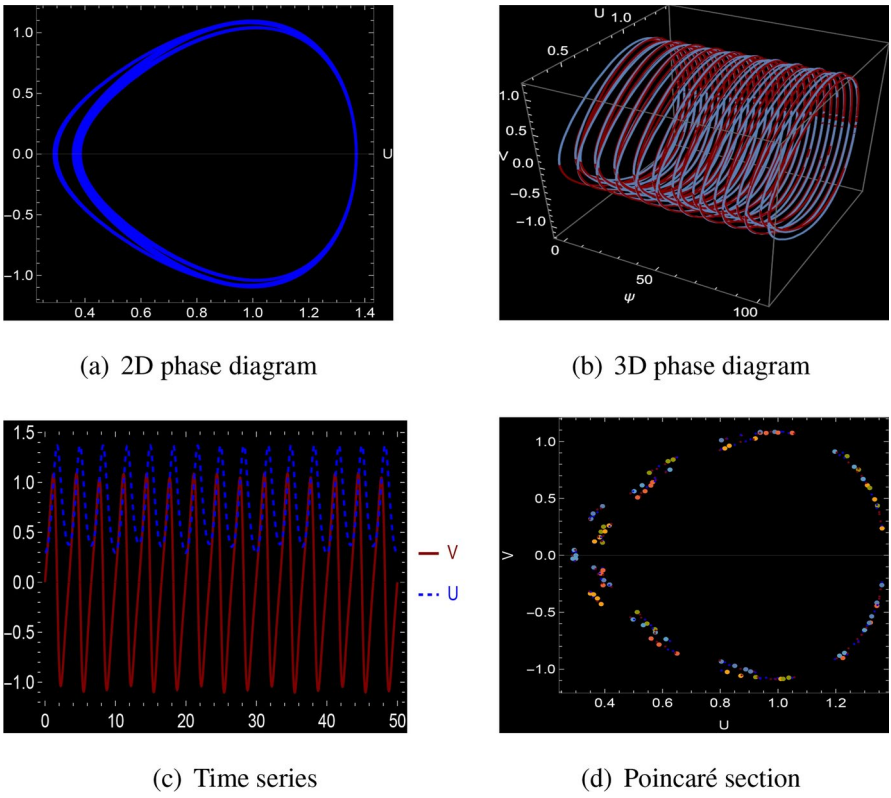

(a) 2D phase diagram

(b) 3D phase diagram

(c) Time series

(d) Poincaré section

Fig. 3 The chaotic behaviors of system (5.1)

Figure 3 examines the system with the parameters $G_1 = -3$,$G_2 = -3$, $\delta = 0.1$, and $\sigma = \pi$. The 2D and 3D phase diagrams in (a) and (b) reveal chaotic dynamics, which are further supported by the time series in (c). The Poincaré sections in (d) demonstrates the absence of quasi-periodic structures, confirming that the system remains within a chaotic regime under these conditions.

Figure 4 presents the system with the parameters $G_1 = -3$, $G_2 = -3$, $\delta = 0.1$, and $\sigma = \frac{\pi}{6}$. The phase diagrams in (a) and (b) highlight the chaotic structure of the system. Furthermore, the time series in (c) and the Poincaré sections in (d) reinforce this chaotic behavior.

Figure 5 investigates the system with parameters $G_1 = 1.33$, $G_2 = 12$, derived from $c = 0.5, m = 3; n = 1$, $\delta = 1$, and $\sigma = \pi$, which result in quasi-periodic structures. The 2D and 3D phase diagrams in (a) and (b) exhibit closed curves, indicating quasi-periodic dynamics. This behavior is further corroborated by the ordered patterns observed in the time series in (c) and the Poincaré sections in (d).

Figure 6 analyzes the system with parameters $G_1 = 1.33$, $G_2 = 12$, $\delta = 1$, and $\sigma = \frac{\pi}{6}$. The 2D and 3D phase diagrams in (a) and (b) clearly demonstrate quasi-periodic behavior. This observation is further supported by the time series in (c) and the regular patterns evident in the Poincaré sections in (d).

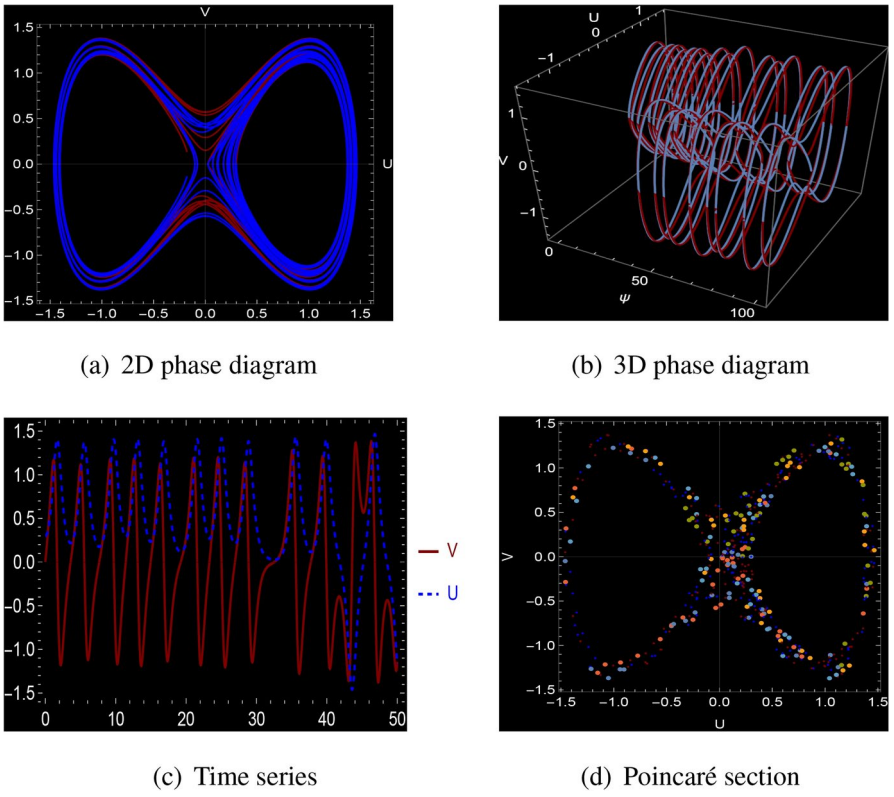

(a) 2D phase diagram

(b) 3D phase diagram

(c) Time series

(d) Poincaré section

Fig. 4 The chaotic behaviors of system (5.1)

Figure 7 explores the system with parameters $G_1 = 1.33$, $G_2 = 12$, $\delta = 7$, and $\sigma = 0.5$. The 2D and 3D phase diagrams in (a) and (b) depict chaotic behavior, as evidenced by the lack of closed curves and the irregular trajectories. The time series in (c) shows irregular oscillations, which are indicative of chaotic dynamics. Additionally, the Poincaré sections in (d) exhibits a scattered distribution of points, further confirming that the system operates within a chaotic regime under these conditions.

Figure 8 examines the system with parameters $G_1 = 1.33$, $G_2 = 12$, $\delta = 7$, and $\sigma = 0.9$. The 2D and 3D phase diagrams in (a) and (b), along with the time series in (c) and the Poincaré sections in (d), collectively demonstrate that the system is entirely chaotic under these conditions.

Remark 2 The bifurcation behavior of the system described by the system (5.1) is significantly influenced by the parameters σ and δ.

Effect of σ on the system dynamics. Figure 9 illustrates how the bifurcation patterns in the $\delta - r$ plane change for $\sigma = 0.8$, $\sigma = 1$, and $\sigma = 1.2$ while keeping $G_1 = -3$ and $G_2 = -3$. The results indicate that:

- For $\sigma = 0.8$, the system exhibits quasi-periodic solutions for small δ values, tran-

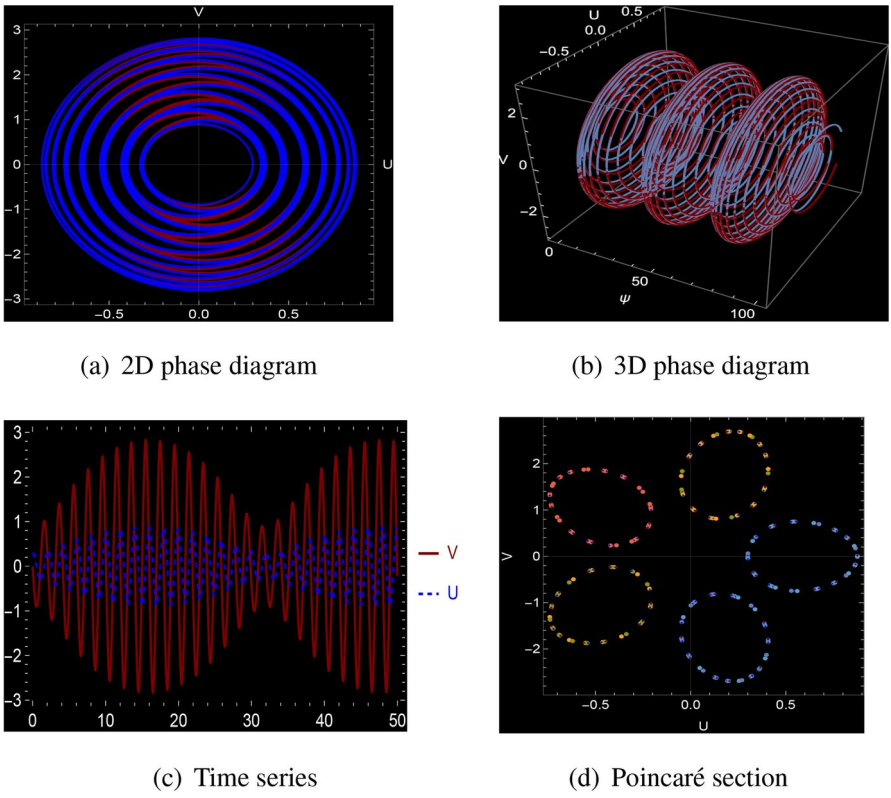

(a) 2D phase diagram

(b) 3D phase diagram

(c) Time series

(d) Poincaré section

Fig. 5 The chaotic behaviors of system (5.1)

sitioning to chaos as δ increases.

- For $\sigma = 1$, the chaotic behavior emerges at smaller δ values compared to $\sigma = 0.8$, with chaos dominating over a broader range.
- For $\sigma = 1.2$, the system displays complex chaotic behavior over a wide range of δ, where periodic behavior is nearly absent.

Effect of δ on the system dynamics. Figure 10 presents the bifurcation patterns in the $\sigma - r$ plane for different δ values. The observations are as follows:

- For $\delta = 0.033$, the system predominantly exhibits periodic behavior for small σ, while chaos emerges in a limited range as σ increases.
- For $\delta = 0.33$, the chaotic regime extends over a broader σ range, indicating the system's increased sensitivity to external forces.
- For $\delta = 0.91$, the system demonstrates highly complex dynamics, with widespread chaotic behavior and multiple solution branches forming at larger σ values.

These findings highlight the critical role of σ and δ in shaping the system's bifurcation structure and dynamic transitions.

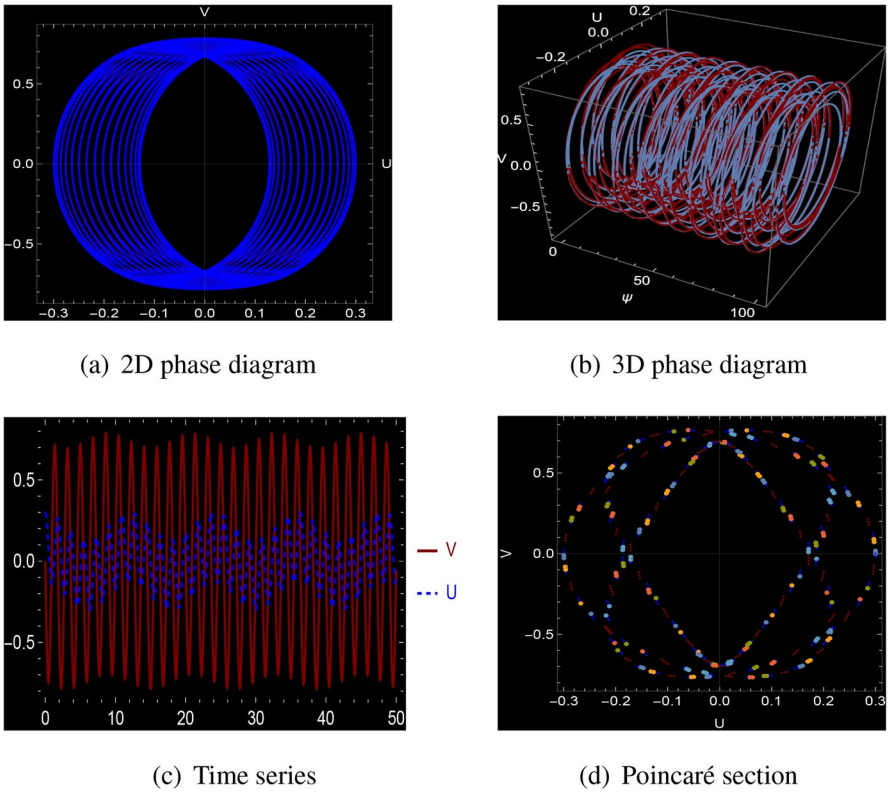

(a) 2D phase diagram (b) 3D phase diagram

(c) Time series (d) Poincaré section

Fig. 6 The chaotic behaviors of system (5.1)

6 Sensitivity Analysis

The sensitivity of systems to initial conditions plays a crucial role in understanding dynamic behaviors. Even minor variations in the initial values can lead to significant differences in the system's behavior. This highlights that minor adjustments in initial conditions can have a substantial impact on the system's long-term dynamics. In this section, the sensitivity analysis of the system under three different boundary conditions is examined. Figure (11) illustrates the behaviors exhibited by the system under these distinct scenarios. The results clearly demonstrate how changes in external constraints or initial parameters influence the system's trajectory and stability. This analysis underscores the critical role of boundary conditions and initial parameters in shaping the overall dynamic structure of the system.

7 Results and Discussion

Numerous studies have been carried out regarding the LGH equation. Baloch et al. [69] investigated analytical solutions of several nonlinear waves for the LGH equation. Ahmad et al. [70] studied the suggested model using two analytical techniques.

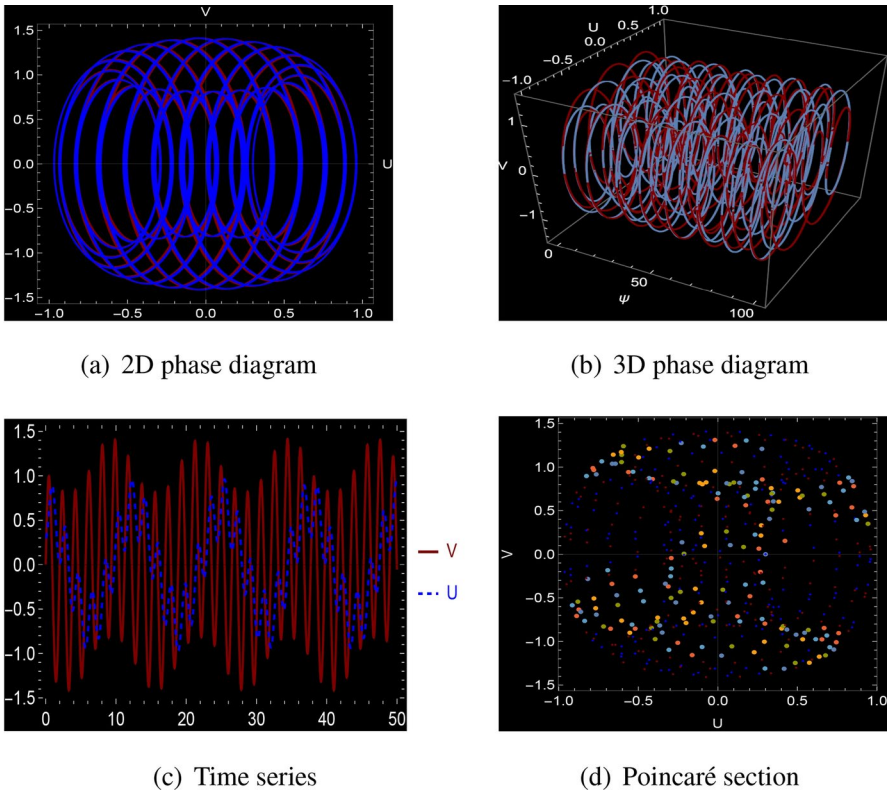

(a) 2D phase diagram

(b) 3D phase diagram

(c) Time series

(d) Poincaré section

Fig. 7 The chaotic behaviors of system (5.1)

Iqbal et al. [71] investigated the optical soliton solution of the LGH equation using the auxiliary equation approach. Unal [72] investigated the analytical solutions of the LGH equation utilizing Jacobi elliptic functions. In this paper, we extract various soliton solutions for the proposed equation using two effective techniques. This section employs contour plots and two- and three-dimensional visualizations to explain the obtained results in detail. Specific waveform solutions, such as kink, anti-kink, bell, anti-bell, periodic, and others, can be created from generic solutions by changing the values of the free parameters. The graphical portrayal of these solutions, which involve a range of arbitrary constants, draws attention to the rich physical phenomena and localized waves of the LGH equation for the proper selection of the corresponding constants. The soliton solutions that have been found are kink and anti-kink-shaped, hyperbolic, periodic, trigonometric, bright and dark, and periodic. There are some physical importance to these solutions. For instance, a dark soliton has less intensity than the background. They are not generated by a traditional pulse and in a continuous time beam, contain no energy. Periodic waves can also be classified as waves whose frequency and wavelength are established by a continuous pattern that repeats. The solution u_3, represents 3D, 2D and contour profiles for the values of parameters $n = 0.5, v = 1.5, \lambda = 1, m = 0.5, \chi = 0.5, g = 5.5, h = 5.5, c = 3$, which is anti-kink shaped soliton shown as in Fig. 12. For the parametric val-

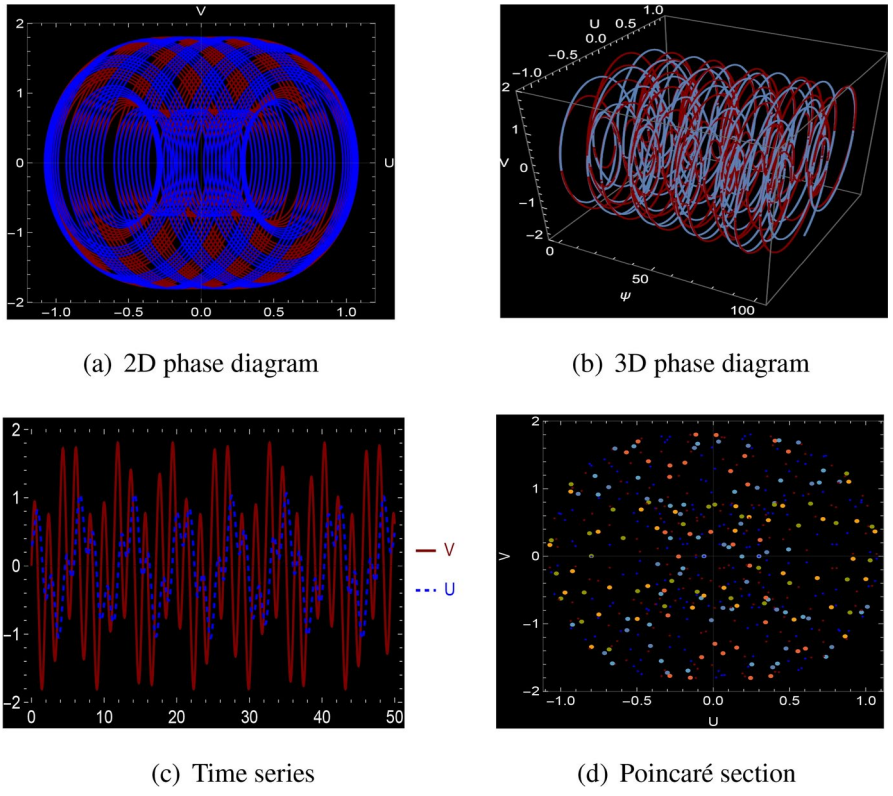

(a) 2D phase diagram (b) 3D phase diagram

(c) Time series (d) Poincaré section

Fig. 8 The chaotic behaviors of system (5.1)

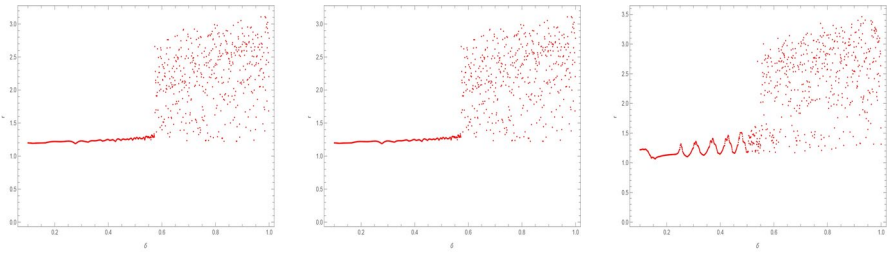

(a) (b) (c)

Fig. 9 The bifurcation behavior of the system (5.1) in the $\delta - r$ plane, with $G_1 = -3$ and $G_2 = -3$, is shown for different values of **(a)** $\sigma = 0.8$, **(b)** $\sigma = 1$, and **(c)** $\sigma = 1.2$

ues $n = -5, v = 0.5, \lambda = -5, m = 0.5, \chi = -0.5, g = -5, h = -0.5, c = 0.9$, the 3D, 2D, and contour plots of the solution u_4 illustrate the periodic soliton with a small wavelength or large frequency, as seen in Fig. 13. For the solutions u_8 and u_{10}, periodic soliton is displayed in Figs. 14 and 15 by considering, $n = 0.5, v = -3.7, \lambda = 0.9, m = -0.5, \chi = 5, g = 05, h = 0.05, c = 0.5$, and $n = -0.5$, $v = -0.05, \lambda = 0.5, m = -0.5, \chi = 0.5, g = 8, h = -0.05, c = 0.5$, respec-

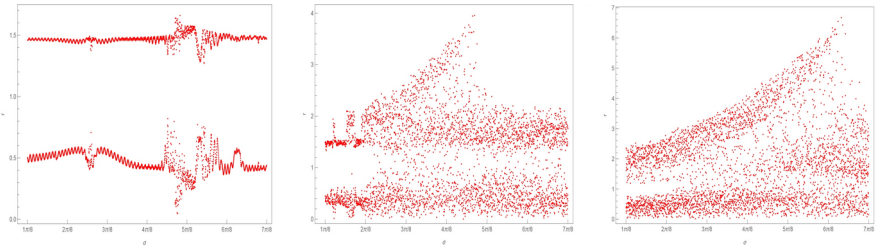

(a) (b) (c)

Fig. 10 The bifurcation behavior of the system (5.1) in the $\sigma - r$ plane, with $G_1 = -3$ and $G_2 = -3$, is shown for different values of (**a**) $\delta = 0.033$, (**b**) $\delta = 0.33$, and (**c**) $\delta = 0.91$

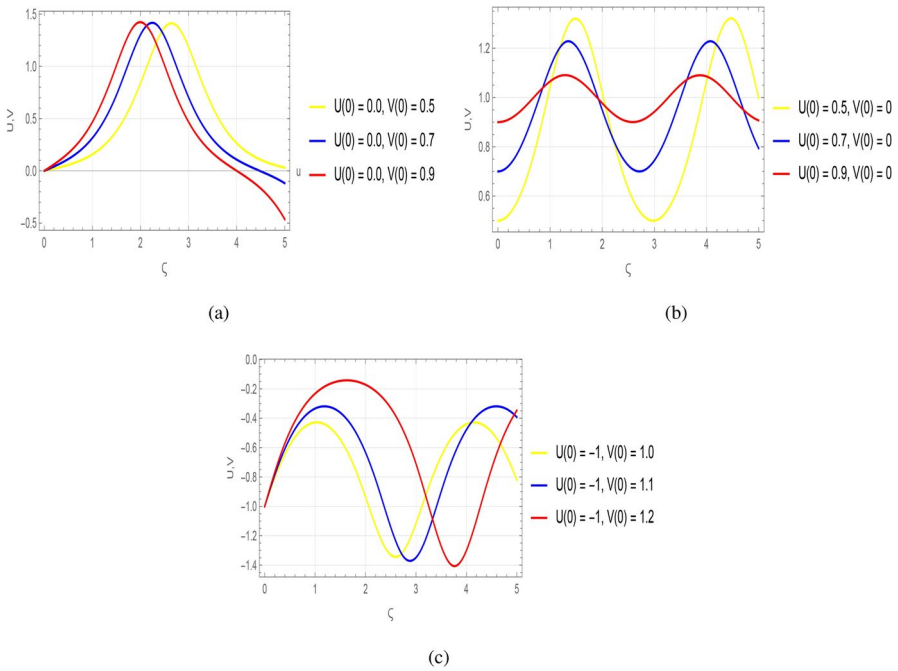

(a) (b)

(c)

Fig. 11 Graph illustrating the sensitivity of the system to initial conditions under different boundary scenarios

tively. Fig. 16 illustrates the bell-shaped soliton solution u_{13}, with parametric values of $n = 0.005, v = 1.5, \lambda = 0.005, m = -5, \chi = 0.05, g = 0.9, h = -0.5, c = 0.9$. The kink shaped soliton is depicted in in Fig. 17 for the solution u_{35}, when $n = 5, v = 1.5, \lambda = 5, m = 0.5, \chi = -5, g = -0.9, h = -0.5, c = -0.9$. Figs. 18 and 19 illustrate bright faces of solutions for Eq. (3.18) and (3.19) for $m = 1.5, n = 0.5, g = -5, h = 1.5, m = 1.5, n = 0.5, g = -5, h = 1.5,$ and $m = 1.5, n = -4.5, g = -15, h = -0.5$, respectively. Fig. 21 represents anti-kink soliton solution for the Eq. (3.25), when $m = -0.9, n = 0.5, g = -0.5, h = 5$. Fig. 22 illustrates the kink-shaped soliton for solution of the Eq. (3.27), taking into account

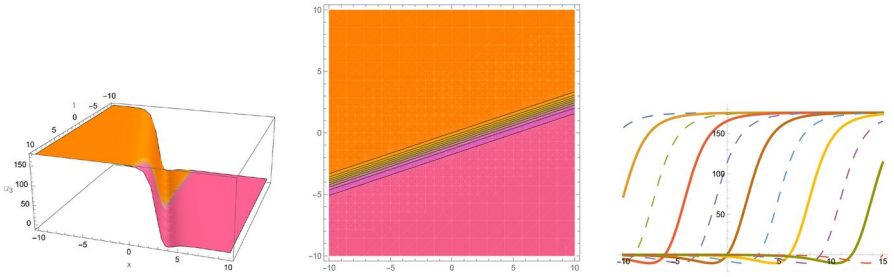

(a) 3D plot (b) contour plot (c) 2D plot

Fig. 12 3D, contour and 2D plots of $u_3(x,t)$ visualizing to anti-kink wave soliton with $n=0.5, v=1.5, \lambda=1, m=0.5, \chi=0.5, g=5.5, h=5.5, c=3$

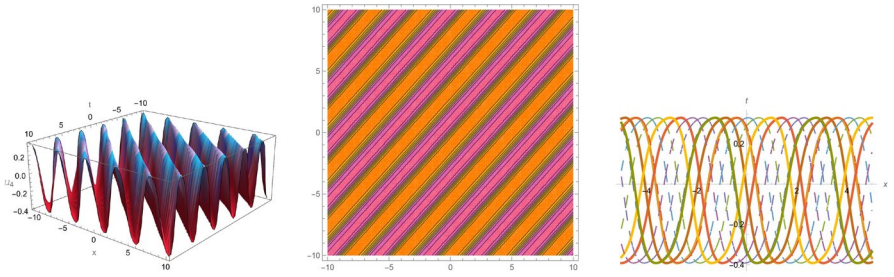

(a) 3D plot (b) contour plot (c) 2D plot

Fig. 13 3D, contour and 2D plots of $u_4(x,t)$ visualizing to periodic wave soliton with $n=-5, v=0.5, \lambda=-5, m=0.5, \chi=-0.5, g=-5, h=-0.5, c=0.9$

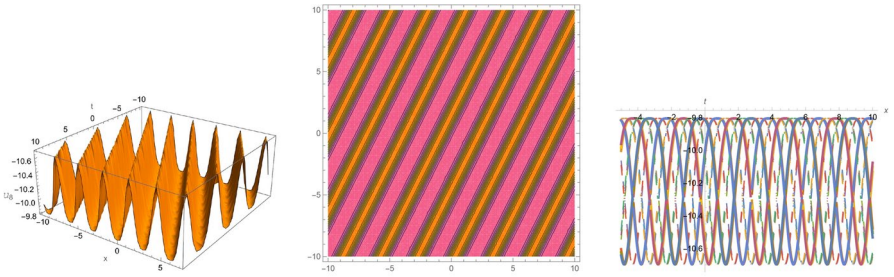

(a) 3D plot (b) contour plot (c) 2D plot

Fig. 14 3D, contour and 2D plots of $u_8(x,t)$ visualizing to periodic wave soliton with $n=0.5, v=-3.7, \lambda=0.9, m=-0.5, \chi=5, g=05, h=0.05, c=0.5$

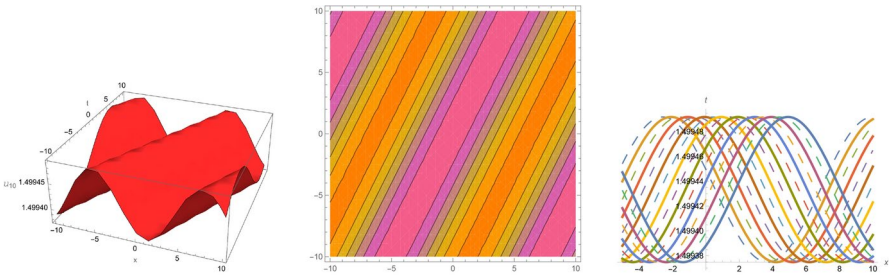

(a) 3D plot (b) contour plot (c) 2D plot

Fig. 15 3D, contour and 2D plots of $u_{10}(x,t)$ visualizing to periodic wave soliton with $n=-0.5, v=-0.05, \lambda=0.5, m=-0.5, \chi=0.5, g=8, h=-0.05, c=0.5$

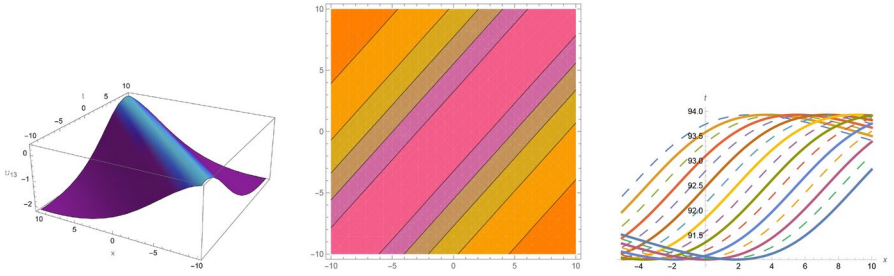

(a) 3D plot (b) contour plot (c) 2D plot

Fig. 16 3D, contour and 2D plots of $u_{13}(x,t)$ visualizing to bell shaped soliton with $n=0.005, v=1.5, \lambda=0.005, m=-5, \chi=0.05, g=0.9, h=-0.5, c=0.9$

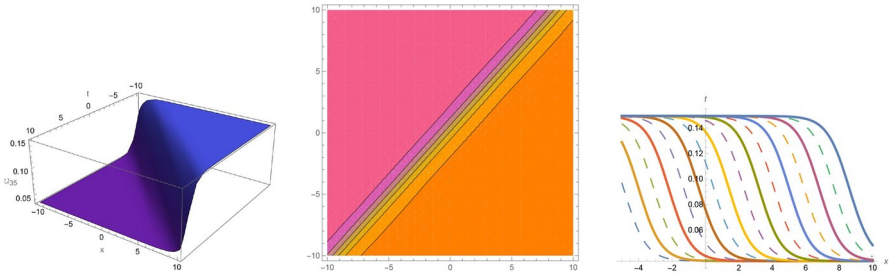

(a) 3D plot (b) contour plot (c) 2D plot

Fig. 17 3D, contour and 2D plots of $u_{35}(x,t)$ visualizing to kink wave soliton with $n=5, v=1.5, \lambda=5, m=0.5, \chi=-5, g=-0.9, h=-0.5, c=0.9$

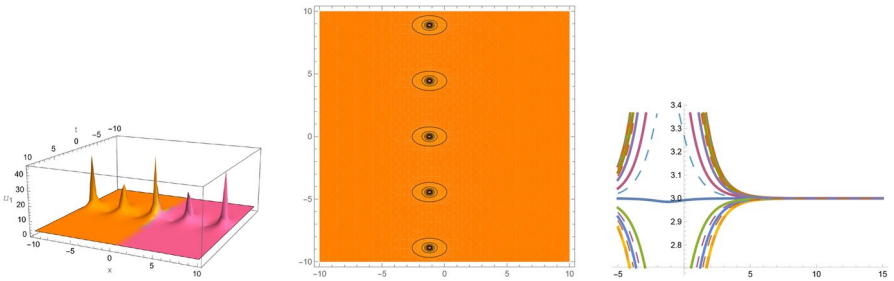

(a) 3D plot (b) contour plot (c) 2D plot

Fig. 18 3D, contour and 2D plots of Eq. (3.18) visualizing to multiple bright faces solitons with $m = 1.5, n = 0.5, g = -5, h = 1.5, m = 1.5, n = 0.5, g = -5, h = 1.5$

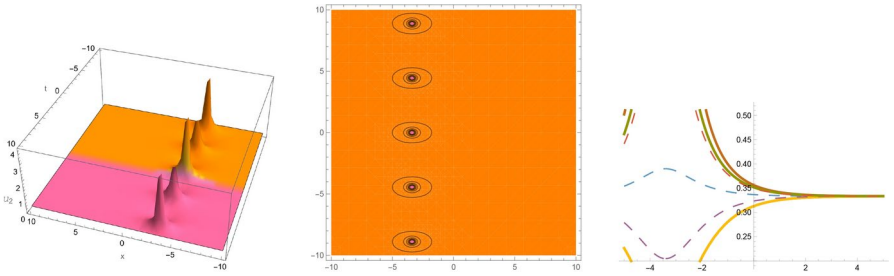

(a) 3D plot (b) contour plot (c) 2D plot

Fig. 19 3D, contour and 2D plots of Eq. (3.19) visualizing to multiple bright faces solitons with $m = 1.5, n = -4.5, g = -15, h = -0.5$

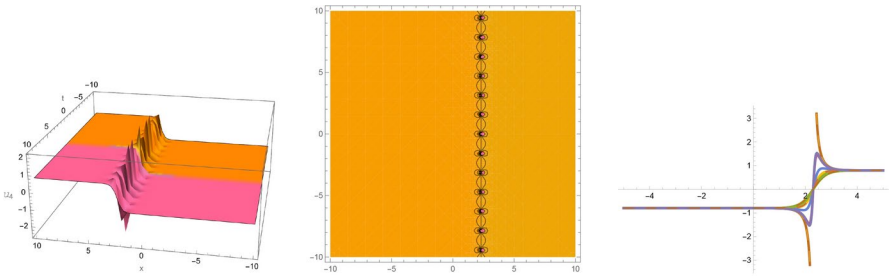

(a) 3D plot (b) contour plot (c) 2D plot

Fig. 20 3D, contour and 2D plots of Eq. (3.23), visualizing to dark-bright singular soliton with $m = 4, n = 5, g = -0.05, h = 5$

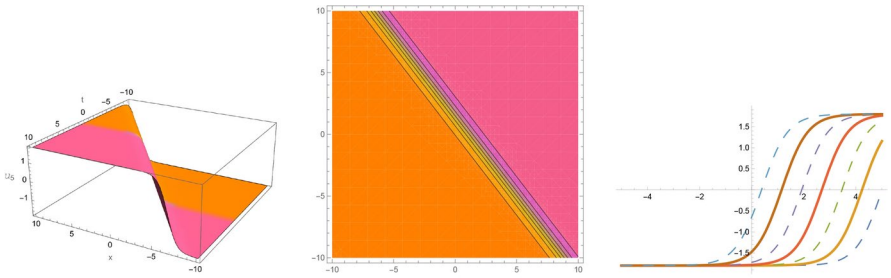

(a) 3D plot (b) contour plot (c) 2D plot

Fig. 21 3D, contour and 2D plots of Eq. (3.25), visualizing to anti-kink wave soliton with $m = -0.9, n = 0.5, g = -0.5, h = 5$

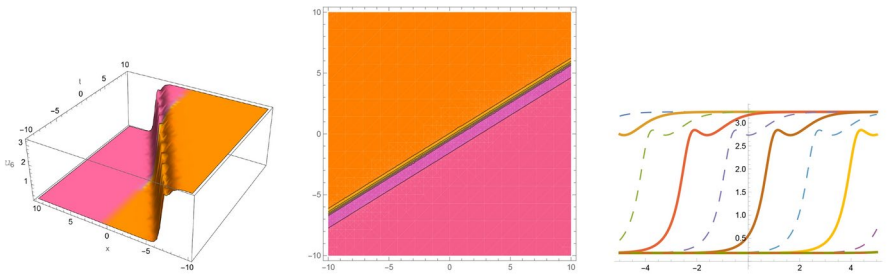

(a) 3D plot (b) contour plot (c) 2D plot

Fig. 22 3D, contour and 2D plots of Eq. (3.27), visualizing to kink wave soliton with $m = 0.9, n = 0.5, g = 0.5, h = 5$

$m = 0.9, n = 0.5, g = 0.5, h = 5$. Fig. 23 presents multiple bright faces of the solution for Eq. (3.37) for $m = 0.9, n = -0.5, B = 0.5, A = -5.5$.

8 Comparison Analysis

This section presents our recent discoveries alongside the contributions of several earlier researchers. While the model has been thoroughly examined in existing literature, our study offers new perspectives on its attributes and dynamics. Asjad et al. studied the LGH equation and obtained several soliton solutions using generalized projective Riccati method [73]. Faridi and AL-Qahatani investigated the same model utilizing Khater method [74]. Rizvi et al. studied the LGH equation with the help of Lie symmetry approach [75]. We present two tables for comparison. In Table 2, we compare our results obtained using modified F-expansion approach and the new extended direct algebraic approach. In Table 3, we compare our results with those reported in the [73].

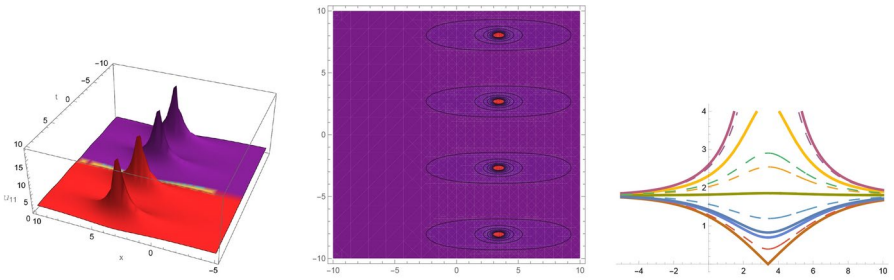

(a) 3D plot (b) contour plot (c) 2D plot

Fig. 23 3D, contour and 2D plots of Eq. (3.37), visualizing to multiple bright faces soliton with with $m = 0.9, n = -0.5, R = 0.5, Q = -5.5$

Table 2 Comparison between modified F-expansion approach and the new extended direct algebraic approach

New extended direct algebraic method	Modified F-expansion method
(i) It provides solutions in the form of rational, hyperbolic trigonometric, and trigonometric functions	(i) It also provides solutions in the form of rational, hyperbolic trigonometric, and trigonometric functions
(ii) It provides 37 solutions	(ii) It provides 11 solutions
(iii) It provides periodic, bright, anti-kink, and kink type solutions	(iii) It provides bright faces, dark-bright singular, anti-kink, and kink type solutions

Table 3 Comparison analysis of our solutions with [73]

Solutions in [73]	Our solutions
(i) Utilized the generalized projective Riccati method	(i) Utilized modified F-expansion approach and the new extended direct algebraic approach
(ii) These solutions include trigonometric and hyperbolic trigonometric solutions	(ii) These solutions included rational, hyperbolic trigonometric, and trigonometric solutions
(iii) Periodic wave solutions, including bright, dark, and kink type, are generated using the proposed method	(iii) Our research results in various solutions such as bell, anti-bell, periodic, kink, anti-kink, and many others
(iv) The sensitivity analysis has been presented	(iv) We conducted an analysis of sensitivity, examined chaotic behavior, and performed bifurcation analysis

9 Conclusions

In this paper, we have effectively used the modified F-expansion approach and the new extended direct algebraic approach to determine the new precise TWs of the LGH equation. As rational, hyperbolic, and trigonometric forms, numerous completely new exact solutions have been found. These techniques provide a systematic and dependable approach for addressing nonlinear fractional governing equations encountered in mathematical physics, as well as for uncovering new exact solutions. However, a limitation of these techniques is their ineffectiveness in scenarios where the highest derivative terms do not uniformly balance with the nonlinear terms. Consequently, our forthcoming research will aim to enhance the applicability of the

methods, particularly for highly nonlinear models and those characterized by variable coefficients and variable order fractional partial differential equations. By setting the parameters to a particular value under constrained conditions, various solutions to the LGH equation are shown in 3D, contour and 2D plots to describe the physical phenomena. With the aid of the computing program Mathematica, the algebraic calculations and visual depictions of the derived solutions for different parameter values are given in this article. Furthermore, the study highlights the impact of the perturbation term on the dynamic behavior of the system, as examined through 2D phase portraits, 3D visualizations, Poincaré sections, and time series. These methods effectively reveal the transitions between periodic, quasi-periodic, and chaotic regimes, emphasizing the critical role of perturbations in shaping the system's behavior. The graphical analyses also demonstrate the system's sensitivity to initial conditions, showing how minor variations can lead to significant differences in the dynamics. These analyses provide deep insights into the system's response under varying conditions, showcasing the significance of nonlinear interactions and external periodic forces in driving complex chaotic dynamics.

Acknowledgements The authors extend their appreciation to Taif university, Saudi Arabia for supporting this work through project number (TU-DSPP-2024-84).

Author Contributions Conceptualization: A.G. and I.S.; Data curation: A.M. and R.Z.; Formal analysis: U.D., K.M., and I.S.; Software: S.B., U.D., and K.M.; Validation: A.G. and I.S.; Writing - original draft: K.M. and S.B.; Writing - review editing: R.Z. and A.M.; All authors have read and agreed to the published version of the manuscript.

Funding This research was funded by Taif University, Saudi Arabia Project number (TU-DSPP-2024-84)

Data Availability Data will be provided to the corresponding author upon request.

Declarations

Conflict of interest The authors declare no conflict of interest.

Ethical Approval All the authors demonstrating that they have adhered to the accepted ethical standards of a genuine research study.

Consent to Participate Being the corresponding author, I have consent to participate of all the authors in this research work.

Consent to Publish All the authors are agreed to publish this research work.

References

1. Osman, M.S., Rezazadeh, H., Eslami, M., Neirameh, A., Mirzazadeh, M.: Analytical study of solitons to benjamin-bona-mahony-peregrine equation with power law nonlinearity by using three methods. University Politehnica of Bucharest Scientific Bulletin-Series A-Applied Mathematics and Physics **80**(4), 267–278 (2018)
2. Osman, M.S., Machado, J.A.T.: The dynamical behavior of mixed-type soliton solutions described by (2+ 1)-dimensional Bogoyavlensky-Konopelchenko equation with variable coefficients. Journal of Electromagnetic Waves and Applications **32**(11), 1457–1464 (2018)
3. Zhao, X.H., Tian, B., Chai, J., Wu, X.Y., Guo, Y.J.: Multi-soliton interaction of a generalized Schrädinger-Boussinesq system in a magnetized plasma. The European Physical Journal Plus **132**, 1–9 (2017)
4. Infeld, E., Rowlands, G.: Nonlinear waves, solitons and chaos. Cambridge University Press (2000)
5. Biswas, A., Milovic, D., Ranasinghe, A.: Solitary waves of Boussinesq equation in a power law media. Communications in Nonlinear Science and Numerical Simulation **14**(11), 3738–3742 (2009)
6. Ebadi, G., Kara, A.H., Petkovic, M.D., Yildirim, A., Biswas, A.: Solitons and conserved quantities of the Ito equation. Proceedings of the Romanian Academy, Series A **13**(3), 215–224 (2012)
7. Sassaman, R., Heidari, A., Biswas, A.: Topological and non-topological solitons of nonlinear Klein-Gordon equations by He's semi-inverse variational principle. Journal of the Franklin Institute **347**(7), 1148–1157 (2010)
8. Abdel-Aty, A.H., Khater, M.M., Attia, R.A., Eleuch, H.: Exact traveling and nano-solitons wave solitons of the ionic waves propagating along microtubules in living cells. Mathematics **8**(5), 697 (2020)
9. Iqbal, I., Rehman, H. U., Mirzazadeh, M., Hashemi, M. S.: Retrieval of optical solitons for nonlinear models with Kudryashov's quintuple power law and dual-form nonlocal nonlinearity. *Optical and Quantum Electronics*, 55**(7**, 588 (2023)
10. Akbulut, A.R.Z.U., Mirzazadeh, M., Hashemi, M.S., Hosseini, K., Salahshour, S., Park, C.: Triki-Biswas model: Its symmetry reduction, Nucci's reduction and conservation laws. International Journal of Modern Physics B **37**(07), 2350063 (2023)
11. Seadawy, A.R., Arnous, A.H., Biswas, A., Belic, M.: Optical solitons with Sasa-Satsuma equation by F-expansion scheme. Optoelectron. Adv. Mater. Rapid Commun **13**(1–2), 31–36 (2019)
12. Asif, N.A., Hammouch, Z., Riaz, M.B., Bulut, H.: Analytical solution of a Maxwell fluid with slip effects in view of the Caputo-Fabrizio derivative. The European Physical Journal Plus **133**, 1–13 (2018)
13. Riaz, M.B., Atangana, A., Jhangeer, A., Tahir, S.: Soliton solutions, soliton-type solutions and rational solutions for the coupled nonlinear Schrädinger equation in magneto-optic waveguides. The European Physical Journal Plus **136**(2), 1–19 (2021)
14. Satsuma, J.: Hirota bilinear method for nonlinear evolution equations. In: Direct and Inverse Methods in Nonlinear Evolution Equations: Lectures Given at the CIME Summer School Held in Cetraro, Italy, September 5–12, 1999, pp. 171–222. Berlin, Heidelberg, Springer, Berlin Heidelberg (2003)
15. Yépez-Martínez, H., Gómez-Aguilar, J.F.: Local M-derivative of order α and the modified expansion function method applied to the longitudinal wave equation in a magneto electro-elastic circular rod. Optical and Quantum Electronics **50**(10), 375 (2018)
16. Wazwaz, A.M.: A sine-cosine method for handlingnonlinear wave equations. Mathematical and Computer modelling **40**(5–6), 499–508 (2004)
17. Malfliet, W.: The tanh method: a tool for solving certain classes of nonlinear evolution and wave equations. Journal of Computational and Applied Mathematics **164**, 529–541 (2004)
18. Aksoy, E., Kaplan, M., Bekir, A.: Exponential rational function method for space-time fractional differential equations. Waves in random and complex media **26**(2), 142–151 (2016)
19. Kumar, D., Hosseini, K., Samadani, F.: The sine-Gordon expansion method to look for the traveling wave solutions of the Tzitzéica type equations in nonlinear optics. Optik **149**, 439–446 (2017)
20. Demirbilek, U., Mamedov, K.R.: Application of IBSEF Method to Chaffee-Infante equation in (1+ 1) and (2+ 1) dimensions. Computational Mathematics and Mathematical Physics **63**(8), 1444–1451 (2023)
21. Demirbilek, U., Nadeem, M., Çelik, F. M., Bulut, H., Şenol, M.: Generalized extended (2+ 1)-dimensional Kadomtsev-Petviashvili equation in fluid dynamics: analytical solutions, sensitivity and stability analysis. Nonlinear Dynamics, 1-16 (2024)

22. Şenol, M., Gençyiğit, M., Demirbilek, U., Akinyemi, L., Rezazadeh, H.: New analytical wave structures of the (3+ 1)-dimensional extended modified Ito equation of seventh-order. Journal of Applied Mathematics and Computing **70**(3), 2079–2095 (2024)
23. Tariq, H., Ashraf, H., Rezazadeh, H., Demirbilek, U.: Travelling wave solutions of nonlinear conformable Bogoyavlenskii equations via two powerful analytical approaches. Applied Mathematics-A Journal of Chinese Universities **39**(3), 502–518 (2024)
24. Parkes, E.J.: Observations on the tanh-coth expansion method for finding solutions to nonlinear evolution equations. Applied Mathematics and Computation **217**(4), 1749–1754 (2010)
25. Zayed, E. M.: Equivalence of The $\left(\frac{G'}{G}\right)$-expansion Method and The Tanh-Coth Function Method. *In AIP Conference Proceedings (Vol. 1281, No. 1, pp. 2225-2228)*. American Institute of Physics (2010)
26. Lu, B.: The first integral method for some time fractional differential equations. Journal of Mathematical Analysis and Applications **395**(2), 684–693 (2012)
27. Taghizadeh, N., Mirzazadeh, M., Tascan, F.: The first-integral method applied to the Eckhaus equation. Applied Mathematics Letters **25**(5), 798–802 (2012)
28. Rezazadeh, H., Korkmaz, A., Eslami, M., Mirhosseini-Alizamini, S.M.: A large family of optical solutions to Kundu-Eckhaus model by a new auxiliary equation method. Optical and Quantum Electronics **51**, 1–12 (2019)
29. Zhang, S.: A generalized new auxiliary equation method and its application to the (2+ 1)-dimensional breaking soliton equations. Applied mathematics and computation **190**(1), 510–516 (2007)
30. Kopçasız, B., Yaşar, E.: Inquisition of optical soliton structure and qualitative analysis for the complex-coupled Kuralay system. Modern Physics Letters B, 2450512 (2024)
31. Jawad, A.J.A.M., Petković, M.D., Biswas, A.: Modified simple equation method for nonlinear evolution equations. Applied Mathematics and Computation **217**(2), 869–877 (2010)
32. Zayed, E.M.: A note on the modified simple equation method applied to Sharma-Tasso-Olver equation. Applied Mathematics and Computation **218**(7), 3962–3964 (2011)
33. Mracek, C.P., Cloutier, J.R.: Control designs for the nonlinear benchmark problem via the state-dependent Riccati equation method. International Journal of robust and nonlinear control **8**(4–5), 401–433 (1998)
34. Yong, C., Biao, L., Hong-Qing, Z.: Generalized Riccati equation expansion method and its application to the Bogoyavlenskii's generalized breaking soliton equation. Chinese Physics **12**(9), 940 (2003)
35. Kopçasız, B.: Unveiling New Exact Solutions of the Complex-Coupled Kuralay System Using the Generalized Riccati Equation Mapping Method. Journal of Mathematical Sciences and Modelling **7**(3), 146–156 (2024)
36. Mirhosseini-Alizamini, S.M., Rezazadeh, H., Eslami, M., Mirzazadeh, M., Korkmaz, A.: New extended direct algebraic method for the Tzitzica type evolution equations arising in nonlinear optics. Computational Methods for Differential Equations **8**(1), 28–53 (2020)
37. Vahidi, J., Zabihi, A., Rezazadeh, H., Ansari, R.: New extended direct algebraic method for the resonant nonlinear Schrädinger equation with Kerr law nonlinearity. Optik **227**, 165936 (2021)
38. Kopçasız, B., Yaşar, E.: Novel exact solutions and bifurcation analysis to dual-mode nonlinear Schrädinger equation. Journal of Ocean Engineering and Science (2022)
39. Barman, H.K., Islam, M.E., Akbar, M.A.: A study on the compatibility of the generalized Kudryashov method to determine wave solutions. Propulsion and Power Research **10**(1), 95–105 (2021)
40. Ryabov, P.N., Sinelshchikov, D.I., Kochanov, M.B.: Application of the Kudryashov method for finding exact solutions of the high order nonlinear evolution equations. Applied Mathematics and Computation **218**(7), 3965–3972 (2011)
41. Shakeel, M., Alaoui, M. K., Zidan, A. M., Shah, N. A.: Closed form solutions for the generalized fifth-order KDV equation by using the modified exp-function method. *Journal of Ocean Engineering and Science* (2022)
42. Heris, J. M., Bagheri, M.: Exact Solutions for the Modified KdV and the Generalized KdV Equations via Exp-Function Method. *Journal of Mathematical Extension* (2010)
43. Lamb, G.L., Jr.: Bäcklund transformations for certain nonlinear evolution equations. Journal of Mathematical Physics **15**(12), 2157–2165 (1974)
44. Vakhnenko, V.O., Parkes, E.J., Morrison, A.J.: A Bäcklund transformation and the inverse scattering transform method for the generalised Vakhnenko equation. Chaos, Solitons & Fractals **17**(4), 683–692 (2003)

45. Abdou, M.A., Elhanbaly, A.: Construction of periodic and solitary wave solutions by the extended Jacobi elliptic function expansion method. Communications in Nonlinear Science and Numerical Simulation **12**(7), 1229–1241 (2007)
46. Ali, A.T.: New generalized Jacobi elliptic function rational expansion method. Journal of computational and applied mathematics **235**(14), 4117–4127 (2011)
47. Khater, M., Anwar, S., Tariq, K. U., Mohamed, M. S.: Some optical soliton solutions to the perturbed nonlinear Schrädinger equation by modified Khater method. *AIP Advances*, 11**(2)** (2021)
48. Li, J., Qiu, Y., Lu, D., Attia, R.A., Khater, M.: Study on the solitary wave solutions of the ionic currents on microtubules equation by using the modified Khater method. Thermal Science **23**(Suppl. 6), 2053–2062 (2019)
49. Kopçasız, B., Yaşar, E.: M-truncated fractional form of the perturbed Chen-Lee-Liu equation: optical solitons, bifurcation, sensitivity analysis, and chaotic behaviors. Optical and Quantum Electronics **56**(7), 1202 (2024)
50. Kopçasız, B.: Qualitative analysis and optical soliton solutions galore: scrutinizing the (2+ 1)-dimensional complex modified Korteweg-de Vries system. Nonlinear Dynamics **112**(23), 21321–21341 (2024)
51. Jhangeer, A., Ansari, A.R., Imran, M., Riaz, M.B., Talafha, A.M.: Application of propagating solitons to Ivancevic option pricing governing model and construction of first integral by Nucci's direct reduction approach. Ain Shams Engineering Journal **15**(4), 102615 (2024)
52. Ansari, A.R., Jhangeer, A., Imran, M., Alsubaie, A.S.A., Inc, M.: Multi-dimensional phase portraits of stochastic fractional derivatives for nonlinear dynamical systems with solitary wave formation. Optical and Quantum Electronics **56**(5), 823 (2024)
53. Jamal, T., Jhangeer, A., Hussain, M.Z.: An anatomization of pulse solitons of nerve impulse model via phase portraits, chaos and sensitivity analysis. Chinese Journal of Physics **87**, 496–509 (2024)
54. Riaz, M.B., Kazmi, S.S., Jhangeer, A., Martinovic, J.: Unveiling solitons and dynamic patterns for a (3+ 1)-dimensional model describing nonlinear wave motion. AIMS Math. **9**(8), 20390–20412 (2024)
55. Jhangeer, A., Ansari, A.R., Imran, M., Riaz, M.B.: Lie symmetry analysis, and traveling wave patterns arising the model of transmission lines. AIMS Mathematics **9**(7), 18013–18033 (2024)
56. Khan, A.Q., Akhtar, T., Jhangeer, A., Riaz, M.B.: Codimension-two bifurcation analysis at an endemic equilibrium state of a discrete epidemic model. AIMS Mathematics **9**(5), 13006–13027 (2024)
57. Hu, W.P., Deng, Z.C., Han, S.M., Fa, W.: Multi-symplectic Runge-Kutta methods for Landau-Ginzburg-Higgs equation. Applied Mathematics and Mechanics **30**(8), 1027–1034 (2009)
58. Lyu, X., Wang, X., Qi, C., Sun, R.: Characteristics of cavity dynamics, forces, and trajectories on vertical water entries with two spheres side-by-side. *Physics of Fluids*, 35**(9)** (2023)
59. Yang, D., Cui, Z., Sheng, H., Chen, R., Cong, R., Wang, S., Xiong, Z.: An occlusion and noise-aware stereo framework based on light field imaging for robust disparity estimation. *IEEE Transactions on Computers* (2023)
60. Xia, F.L., Jarad, F., Hashemi, M.S., Riaz, M.B.: A reduction technique to solve the generalized nonlinear dispersive mK (m, n) equation with new local derivative. Results in Physics **38**, 105512 (2022)
61. Hashemi, M.S., Mirzazadeh, M.: Optical solitons of the perturbed nonlinear Schrädinger equation using Lie symmetry method. Optik **281**, 170816 (2023)
62. Bekir, A., Unsal, O.: Exact solutions for a class of nonlinear wave equations by using first integral method. International Journal of Nonlinear Science **15**(2), 99–110 (2013)
63. Iftikhar, A., Ghafoor, A., Zubair, T., Firdous, S., Mohyud-Din, S.T.: Solutions of (2+ 1) Dimensional Generalized KdV, Sin Gordon and Landau-Ginzburg-Higgs Equations. Scientific Research and Essays **8**(28), 1349–1359 (2013)
64. Islam, M.E., Akbar, M.A.: Stable wave solutions to the Landau-Ginzburg-Higgs equation and the modified equal width wave equation using the IBSEF method. Arab Journal of Basic and Applied Sciences **27**(1), 270–278 (2020)
65. Siddique, I., Mehdi, K.B., Jarad, F., Elbrolosy, M.E., Elmandouh, A.A.: Novel precise solutions and bifurcation of traveling wave solutions for the nonlinear fractional (3+ 1)-dimensional WBBM equation. International Journal of Modern Physics B **37**(02), 2350011 (2023)
66. Siddique, I., Mehdi, K.B., Akbar, M.A., Khalifa, H.A.E.W., Zafar, A.: Diverse Exact Soliton Solutions of the Time Fractional Clannish Random Walker's Parabolic Equation via Dual Novel Techniques. Journal of Function Spaces **2022**(1), 1680560 (2022)

67. Sağlam, F.N.K., Kopçasız, B., Tariq, K.U.: Optical Solitons and Dynamical Structures for the Zig-zag Optical Lattices in Quantum Physics. International Journal of Theoretical Physics **64**(2), 1–20 (2025)
68. Kopçasız, B., Sağlam, F. N. K., Malik, S.: Exact soliton solutions for the (n+ 1)-dimensional generalized Kadomtsev-Petviashvili equation via two novel methods. International Journal of Geometric Methods in Modern Physics, 2550105 (2025)
69. Baloch, S.A., Abbas, M., Nazir, T., Hamed, Y.S.: Lump, periodic, multi-waves and interaction solutions to non-linear Landau-Ginzburg-Higgs model. Optical and Quantum Electronics **56**(8), 1345 (2024)
70. Ahmad, S., Mahmoud, E.E., Saifullah, S., Ullah, A., Ahmad, S., Akgül, A., El Din, S.M.: New waves solutions of a nonlinear Landau-Ginzburg-Higgs equation: The Sardar-subequation and energy balance approaches. Results in Physics **51**, 106736 (2023)
71. Iqbal, M., Faridi, W.A., Ali, R., Seadawy, A.R., Rajhi, A.A., Anqi, A.E., Alamri, S.: Dynamical study of optical soliton structure to the nonlinear Landau-Ginzburg-Higgs equation through computational simulation. Optical and Quantum Electronics **56**(7), 1192 (2024)
72. Unal, S.C.: Exact solutions of the Landau-Ginzburg-Higgs equation utilizing the Jacobi elliptic functions. Optical and Quantum Electronics **56**(6), 1–27 (2024)
73. Asjad, M.I., Majid, S.Z., Faridi, W.A., Eldin, S.M.: Sensitive analysis of soliton solutions of nonlinear Landau-Ginzburg-Higgs equation with generalized projective Riccati method. AIMS Math. **8**(5), 10210–10227 (2023)
74. Faridi, W.A., AlQahtani, S.A.: The formation of invariant exact optical soliton solutions of Landau-Ginzburg-Higgs equation via Khater analytical approach. International Journal of Theoretical Physics **63**(2), 31 (2024)
75. Rizvi, S.T.R., Ali, K., Aziz, N., Seadawy, A.R.: Lie symmetry analysis, conservation laws and soliton solutions by complete discrimination system for polynomial approach of Landau Ginzburg Higgs equation along with its stability analysis. Optik **300**, 171675 (2024)

Authors and Affiliations

Khush Bukht Mehdi[1] · Abd Allah A. Mousa[2] · Sajawal Abbas Baloch[3] · Ulviye Demirbilek[4] · Abdullatif Ghallab[5] · Imran Siddique[3,6] · Rana Muhammad Zulqarnain[7]

✉ Abdullatif Ghallab
ghallab@ust.edu.ye

Khush Bukht Mehdi
bkmehdi786@gmail.com

Abd Allah A. Mousa
a.mousa@tu.edu.sa

Sajawal Abbas Baloch
sajawalabbasbaloch@gmail.com

Ulviye Demirbilek
udemirbilek@mersin.edu.tr

Imran Siddique
imransmsrazi@gmail.com

Rana Muhammad Zulqarnain
ranazulqarnain7777@gmail.com

[1] Department of Mathematics, University of Management and Technology, Lahore 54770, Pakistan

[2] Department of Mathematics and Statistics, College of Science, Taif University, P.O. Box 11099, Taif 21944, Saudi Arabia

[3] Department of Mathematics, University of Sargodha, 40100 Sargodha, Pakistan

[4] Department of Mathematics, Mersin University, Mersin, Turkey

[5] Department of Computer Science, University of Science and Technology, P.O. Box: 13064, Sana'a, Yemen

[6] Mathematics in Applied Sciences and Engineering Research Group, Scientific Research Center, Al-Ayen University, 64001 Nasiriyah, Iraq

[7] Department of Mathematics, Saveetha School of Engineering, SIMATS, Thandalam, Chennai, Tamilnadu 602105, India